Stabilization of Multimode Schrödinger Cat States Via Normal-Mode Dissipation Engineering

Petr Zapletal[1,2,*], Andreas Nunnenkamp[4,3,2] and Matteo Brunelli[2,5]

[1]*Department of Physics, Friedrich-Alexander University Erlangen-Nürnberg (FAU), Erlangen 91058, Germany*

[2]*Cavendish Laboratory, University of Cambridge, Cambridge CB3 0HE, United Kingdom*

[3]*School of Physics and Astronomy and Centre for the Mathematics and Theoretical Physics of Quantum Non-Equilibrium Systems, University of Nottingham, Nottingham NG7 2RD, United Kingdom*

[4]*Faculty of Physics, University of Vienna, Boltzmanngasse 5, 1090 Vienna, Austria*

[5]*Department of Physics, University of Basel, Klingelbergstrasse 82, Basel 4056, Switzerland*

Non-Gaussian quantum states have been deterministically prepared and autonomously stabilized in single- and two-mode circuit quantum electrodynamics architectures via engineered dissipation. However, it is currently unknown how to scale up this technique to multimode non-Gaussian systems. Here, we upgrade dissipation engineering to collective (normal) modes of nonlinear resonator arrays and show how to stabilize multimode Schrödinger cat states. These states are multiphoton and multimode quantum superpositions of coherent states in a single normal mode delocalized over an arbitrary number of cavities. We consider tailored dissipative coupling between resonators that are parametrically driven and feature an on-site nonlinearity, which is either a Kerr-type nonlinearity or an engineered two-photon loss. For both types of nonlinearity, we find the same exact closed-form solutions for the two-dimensional steady-state manifold spanned by superpositions of multimode Schrödinger cat states. We further show that, in the Zeno limit of strong dissipative coupling, the even-parity multimode cat state can be deterministically prepared from the vacuum. Remarkably, engineered two-photon loss gives rise to a fast relaxation toward the steady state, protecting the state preparation against decoherence due to intrinsic single-photon losses and imperfections in tailored dissipative coupling, which sets in at longer times. The relaxation time is independent of system size making the state preparation scalable. Multimode cat states are naturally endowed with a noise bias that increases exponentially with system size and can thus be exploited for enhanced robust encoding of quantum information.

I. INTRODUCTION

Schrödinger cat states—quantum superpositions of macroscopically distinct (or "classical") states—are a fundamental resource for quantum communication [1], quantum metrology [2–4], and quantum computation [5–7]. Recently, the development of bosonic quantum error-correcting codes has led to a surge of interest in exploiting Schrödinger cat states for encoding and manipulating quantum information in a hardware-efficient manner [6–17]. The two-dimensional subspace spanned by superpositions of Schrödinger cat states can be used to

encode quantum information, implementing a so-called cat qubit. Interestingly, such a qubit is naturally endowed with a large noise bias, i.e., the qubit has a single dominant noise channel while all other types of noise are largely suppressed, which offers protection from errors in a quantum memory [8,11], and eases up the requirements of quantum error correction [13] and quantum annealing [18]. The implementation of bias-preserving quantum gates [7,14–16] opens the door for universal fault-tolerant quantum computing based on cat qubits [6]. The potential for applications of Schrödinger cat states further increases when considering extensions to multiple modes. Two-mode Schrödinger cat states, also known as entangled coherent states [19], are a resource for continuous-variable quantum information [20,21] and metrology [22,23]. They have been experimentally prepared using feedback control in superconducting circuits [24]. A unique feature of these states is that they possess non-Gaussian entanglement, which allows circumventing many

---

*petr.zapletal@fau.de

no-go theorems imposed by Gaussian quantum resources [25]. Extending the stabilization of non-Gaussian entangled states—and Schrödinger cat states in particular—to an arbitrary number of modes would render non-Gaussian quantum resources scalable [26].

The widespread application of Schrödinger cat states to photonic quantum technologies is also due to the unique control capabilities available in circuit quantum electrodynamics (circuit QED) architectures, which guarantee unprecedented control of nonlinear interactions and dissipation [27–29]. In this context, a particularly convenient approach is dissipation engineering [30,31], which exploits tailored interactions with a dissipative environment to attain deterministic and robust preparation of desired target states or operations. The dissipative preparation of single-mode Schrödinger cat states using engineered two-photon loss and two-photon (parametric) drive was first envisioned in Ref. [32]. For a circuit QED setup, the autonomous stabilization of a two-dimensional subspace spanned by single-mode cat states has been recently proposed in Ref. [9] and realized in Ref. [10]. It has also been proposed how to generate approximate two-mode Schrödinger cat states via dissipation engineering [33]. However, engineering *multimode* Schrödinger cat states and the stabilization of steady-state manifolds thereof in driven-dissipative parametrically coupled systems have remained an unexplored avenue.

In this work we propose how to dissipatively generate multimode cat states in a scalable fashion and show how to autonomously stabilize a decoherence-free subspace (DFS), which is spanned by multimode Schrödinger cat states. Our approach consists in upgrading dissipation engineering to collective modes (normal modes) of *dissipatively* coupled arrays of nonlinear resonators. We present our ideas in terms of two closely related models that are readily realizable with parametrically driven superconducting circuits. The first model is, as sketched in Fig. 1(a), based on an array of parametrically driven Kerr resonators, also known as Kerr parametric resonators (KPRs). In the second model, the Kerr nonlinearity is replaced by engineered two-photon dissipation, depicted in Fig. 1(b). In both cases, the only source of coupling is provided by engineered nonlocal dissipation connecting neighboring pairs of modes. This kind of nonlocal dissipation has recently been considered in the proposal for the generation of two-mode Schrödinger cat states [33] and in several other contexts, e.g., to realize nonreciprocal photon transport in a pair of modes [31] or in cavity arrays [34,35]. In contrast, the more conventional scenario of arrays of coherently (tunnel-)coupled KPRs has been studied in Refs. [36,37], in connection with the emergence of critical behavior. Fully connected networks of tunnel-coupled KPRs have also been proposed for solving combinatorial optimization problems [38,39].
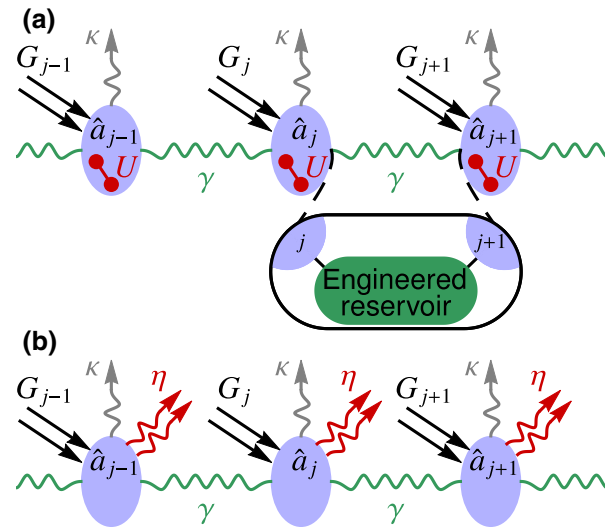

FIG. 1. Two cavity arrays considered for the stabilization of multimode Schrödinger cat states; straight (wiggly) lines represent Hamiltonian (dissipative) contributions. (a) One-dimensional array of N resonators $\hat{a}_j$ with on-site Kerr nonlinearity U, nonlocal dissipation at rate γ, parametric two-photon drive with amplitudes $G_j = Ge^{-i\theta j}$, intrinsic photon loss at rate κ, and periodic boundary conditions $\hat{a}_{N+1} = \hat{a}_1$. The inset shows that nonlocal dissipation is implemented via coupling to an engineered reservoir. Note that each dissipative process (wiggly lines) is due to coupling to an independent reservoir. (b) Alternative model where the Kerr nonlinearity is replaced by local two-photon loss at rate η.

As we will see, the choice of the pairwise dissipative coupling is responsible for the unique features of our model. The idea is simple and yet extremely powerful, as it allows us to select a single normal mode and completely suppress its decay, while all the other normal modes can be heavily damped. The interaction between the (driven) nondissipative normal mode and the other dissipative modes leads to an asymptotically stable Schrödinger cat manifold for the nondissipative mode, which we characterize analytically. Since these cat states are stabilized in a normal mode, they are indeed multimode superpositions delocalized over the entire array. We further show that the stabilization of multimode cat states is robust against intrinsic single-photon loss and imperfections in the dissipative coupling. In particular, the model featuring local two-photon loss [cf. Fig. 1(b)] guarantees a fast relaxation toward the asymptotic manifold, which allows for an efficient steady-state preparation of the even-parity cat state from the vacuum even in the presence of intrinsic single-photon loss. Multimode cat states can be stabilized and prepared in the Zeno limit even in the presence of imperfections in nonlocal dissipation, albeit with decreased fidelity as an additional decoherence channel sets in. The relaxation time toward the Schrödinger cat manifold is independent of system size, making the state preparation

scalable. Crucially, the noise bias of multimode cat states exponentially increases with system size, which can be exploited for realizing a quantum memory with enhanced protection with respect to single-mode implementations.

The remainder of this work is structured as follows. In Sec. II we introduce our first model, namely the Kerr-resonator array of Fig. 1(a). In Sec. III we derive an analytic expression for the steady states of the model, which takes the form of a two-dimensional DFS spanned by even and odd multimode Schrödinger cat states. In Sec. IV we discuss how to target such states, and we show that, for sufficiently strong nonlocal dissipation, the even multimode cat state can be faithfully prepared by initializing the array in the vacuum. In Sec. V we explain this behavior by developing an effective single-mode theory, valid in the Zeno limit of strong nonlocal dissipation. We describe the long-time dynamics of the nondissipative mode and extract an analytical expression of the dissipative gap, dictating the slowest convergence time to the steady state. The expression shows that the requirements of preparing a cat state from the vacuum with near-unit fidelity and guaranteeing a fast convergence cannot be simultaneously satisfied. In Sec. VI we then show how this drawback can be remedied by replacing the Kerr nonlinearity with local two-photon loss as shown in Fig. 1(b). In Sec. VII we account for the effect of unwanted decoherence mechanisms. We include in both models intrinsic single-photon loss, which causes decoherence within the steady-state manifold. In Sec. VIII, we discuss effects of decoherence due to imperfections in nonlocal dissipation. In Sec. IX, we discuss the noise bias of the multimode cat manifold and how it can be exploited for a robust encoding of quantum information. In Sec. X, we estimate experimentally relevant parameters of our model based on state-of-the-art circuit QED technology. Section XI contains concluding remarks and possible directions for future investigation.

II. MODEL

We consider a one-dimensional array of N identical Kerr resonators, as depicted in Fig. 1(a), each subject to a parametric two-photon drive. In a frame rotating at the resonator frequency and for the pump frequency matching twice the resonator frequency, the system is described by the Hamiltonian $\hat{H} = \hat{H}_U + \hat{H}_G$ ($\hbar = 1$), where

$$\hat{H}_U = \sum_{j=1}^{N} U \hat{a}_j^\dagger \hat{a}_j^\dagger \hat{a}_j \hat{a}_j, \qquad (1)$$

$$\hat{H}_G = \sum_{j=1}^{N} [G_j \hat{a}_j^\dagger \hat{a}_j^\dagger + \text{H.c.}], \qquad (2)$$

with U the strength of the Kerr nonlinearity and $G_j = G e^{-i\theta j}$ the amplitude of the two-photon drive at site j

with a phase difference θ between neighboring resonators; without loss of generality, we assume that $G > 0$.

The distinctive feature of our model lies in the coupling between resonators, which is not described by a Hamiltonian term, but has instead a *dissipative* nature, inasmuch as it correlates photon emission events from neighboring resonators. This is formally described by a nonlocal dissipation term in the Lindblad master equation

$$\dot{\hat{\rho}} = -i[\hat{H}, \hat{\rho}] + \gamma \sum_{j=1}^{N} \mathcal{D}[\hat{a}_j - e^{i\phi} \hat{a}_{j+1}]\hat{\rho} = \mathcal{L}\hat{\rho}, \quad (3)$$

where γ is the rate of nonlocal dissipation, $\mathcal{L}$ is the Liouvillian superoperator, and $\mathcal{D}[\hat{O}]\hat{\rho} = \hat{O}\hat{\rho}\hat{O}^\dagger - \frac{1}{2}(\hat{O}^\dagger\hat{O}\hat{\rho} + \hat{\rho}\hat{O}^\dagger\hat{O})$. Loosely speaking, this unconventional dissipator can be interpreted as a dissipative analogue of a hopping term. In fact, it corresponds to indirect hopping via an auxiliary, fast decaying, mode, which acts as an engineered reservoir; see the inset of Fig. 1(a). It can be implemented in different ways, e.g., via coupling the neighboring resonators $\hat{a}_j$ and $\hat{a}_{j+1}$ to a transmission line with respective coupling amplitudes having a relative phase difference ϕ [31,33].

We assume periodic boundary conditions $\hat{a}_{N+1} = \hat{a}_1$. In this case, nonlocal dissipation can be expressed in the plane-wave basis $\hat{b}_k = (1/\sqrt{N}) \sum_{j=1}^{N} e^{ijk}\hat{a}_j$ as

$$\gamma \sum_{j=1}^{N} \mathcal{D}[\hat{a}_j - e^{i\phi} \hat{a}_{j+1}]\hat{\rho} = \sum_{k=1}^{N} \gamma_k \mathcal{D}[\hat{b}_k]\hat{\rho}, \qquad (4)$$

where the rate of dissipation $\gamma_k = 2\gamma[1 - \cos(k - \phi)]$ depends on the quasimomentum k that takes the values $k = (2\pi/N), 2(2\pi/N), \ldots, 2\pi$. From Eq. (4) we see that the effect of engineered nonlocal dissipation is best understood in momentum space, where it takes the form of a nonuniform damping for the normal modes. In particular, the normal mode with $k = \phi$ is a dark mode of the nonlocal dissipator, which does not experience any dissipation as $\gamma_\phi = 0$. Therefore, the relative phase ϕ allows us to select a single *nondissipative normal mode*. This behavior is to be contrasted with intrinsic, i.e., nonengineered, single-photon loss, which instead leads to homogeneous decay of all normal modes. For now we assume that Eq. (4) is the only dissipation channel acting on the system; effects of intrinsic photon loss will be accounted for in Sec. VII.

Writing the Hamiltonian in the plane-wave basis we get

$$\hat{H}_U = \frac{U}{N} \sum_{k_1,k_2,k_3,k_4} \delta_{k_1+k_2,k_3+k_4} \hat{b}_{k_1}^\dagger \hat{b}_{k_2}^\dagger \hat{b}_{k_3} \hat{b}_{k_4}, \qquad (5)$$

$$\hat{H}_G = \sum_k (G \hat{b}_k^\dagger \hat{b}_{\theta-k}^\dagger + \text{H.c.}), \qquad (6)$$

where $\delta_{k_1+k_2,k_3+k_4}$ is the Kronecker delta and the arguments $k_1 + k_2$ and $k_3 + k_4$ are defined modulo 2π. We can see that the Kerr nonlinearity $\hat{H}_U$ corresponds to a four-wave mixing process, which scatters a photon pair k_1 and k_2 to a photon pair k_3 and k_4, conserving the total quasimomentum. The two-photon drive $\hat{H}_G$ corresponds to the creation of a photon pair with a total quasimomentum θ.

III. MULTIMODE DECOHERENCE-FREE SUBSPACE

Our first goal is to characterize the steady states of master equation (3). In particular, we look for steady states in the form of pure states $|\Psi\rangle$, which are referred to as *dark states* [40]. Combining Eqs. (3) and (4) it readily follows that dark states must satisfy the two conditions

$$\hat{b}_k|\Psi\rangle = 0 \quad \text{for all } k \neq \phi, \tag{7}$$

$$\hat{H}|\Psi\rangle = \epsilon|\Psi\rangle. \tag{8}$$

Condition (7) is satisfied if all modes $k \neq \phi$ are in the vacuum, i.e., $|\Psi\rangle = (\bigotimes_{k\neq\phi}|0\rangle_k) \otimes |\psi\rangle_\phi$, from which it is clear that the role of engineered dissipation is to select a single normal mode that is (possibly) populated in the infinite-time limit. Dark state condition (8) can then be written as

$$\sum_k \hat{b}_k^\dagger \hat{b}_{2\phi-k}^\dagger (\hat{b}_\phi^2 - \zeta^2)|\Psi\rangle = \zeta^{*2}\left(\hat{b}_\phi^2 - \frac{\epsilon}{G}\right)|\Psi\rangle, \tag{9}$$

where $\zeta = i\sqrt{NG/U}$ and we hereafter set $\theta = 2\phi$ [41]. For $\epsilon = G\zeta^2$, overall destructive interference is guaranteed if the degenerate photon pairs annihilated in mode ϕ satisfy the condition

$$(\hat{b}_\phi^2 - \zeta^2)|\psi\rangle_\phi = (\hat{b}_\phi - \zeta)(\hat{b}_\phi + \zeta)|\psi\rangle_\phi = 0, \tag{10}$$

in which case both sides of Eq. (9) vanish.

Equation (10) represents a simplified dark state condition. From its factorized form we can deduce that the two coherent states $\hat{b}_\phi|\pm\zeta\rangle_\phi = \pm\zeta|\pm\zeta\rangle_\phi$ and their superpositions are dark states. All possible dark states span a two-dimensional subspace shown in Fig. 2(a), whose basis states are superpositions of coherent states, known as Schrödinger cat states $|\mathcal{C}^\pm\rangle_\phi = \mathcal{N}_\pm(|\zeta\rangle_\phi \pm |-\zeta\rangle_\phi)$, where $\mathcal{N}_\pm = [2(1 \pm e^{-2|\zeta|^2})]^{-1/2}$. Note that the cat states $|\mathcal{C}^\pm\rangle_\phi$ are exactly orthogonal in contrast to the coherent states $|\pm\zeta\rangle_\phi$, which have a finite overlap. For convenience, from now on we drop the subscript ϕ from the state of the nondissipative mode. Because of the linearity of the master equation, incoherent mixtures of dark states are also steady states. All dark states and their incoherent mixtures span a DFS

$$\hat{\rho}_{\text{SS}} = c_{++}|\mathcal{C}^+\rangle\langle\mathcal{C}^+| + c_{--}|\mathcal{C}^-\rangle\langle\mathcal{C}^-|$$
$$+ (c_{+-}|\mathcal{C}^+\rangle\langle\mathcal{C}^-| + \text{H.c.}), \tag{11}$$

where the coefficients c_μ depend on the initial state. Even though steady states that are neither dark states nor their incoherent mixtures can in principle exist [40], we numerically verified that master equation (3) has no steady states lying outside of the DFS (11) (see Appendix A for more details).

Note that DFSs with a similar structure have recently been realized in circuit QED [7,10,14,17,42]. However, compared to these cases, here the crucial difference is that the DFS is spanned by *multimode* Schrödinger cat states. In fact, the ground state of a single nondissipative KPR supports a two-dimensional manifold spanned by *single-mode* cat states of amplitude $\zeta = i\sqrt{G/U}$ [12,43]. The steady state of a parametrically driven resonator with engineered two-photon dissipation (hereafter simply referred to as two-photon driven dissipation) [9] also supports a similar manifold, in this case with amplitude $\zeta = \sqrt{-iG/\eta}$, where η is the rate of two-photon dissipation (see Sec. VI
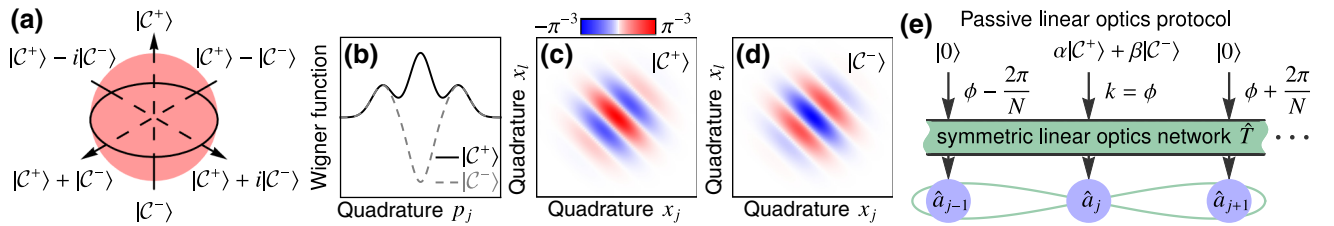

FIG. 2. Multimode decoherence-free subspace. (a) Two-dimensional subspace consisting of dark states of the Kerr-resonator array corresponding to all superpositions of cat states $|\mathcal{C}^\pm\rangle$. (b) The N-mode Wigner function $W(x_1,\ldots,x_N,p_1,\ldots,p_N)$ along $p_j = p_N$ with $x_j = 0$ (for all j) for the even-parity cat state $|\mathcal{C}^+\rangle$ (black solid lines) and for the odd-parity cat state $|\mathcal{C}^-\rangle$ (gray dashed lines) stabilized in the normal mode $\phi = 0$, where $\hat{x}_j \propto \hat{a}_j^\dagger + \hat{a}_j$ and $\hat{p}_j \propto i(\hat{a}_j^\dagger - \hat{a}_j)$ are quadratures of resonator j. Similarly to single-mode cat states, we can see two satellite peaks corresponding to the coherent states $\bigotimes_{j=1}^N |\pm\zeta_j\rangle_j$. (c),(d) Interference fringes of the N-mode Wigner function in the x_j-x_l plane (for any $j \neq l$) for $|\mathcal{C}^+\rangle$ and $|\mathcal{C}^-\rangle$, respectively—a unique feature of multimode cat states absent for single-mode cat states. (e) Mixing of a single-mode cat state with $N - 1$ vacuum states on a symmetric linear optics network that corresponds to expressing the multimode cat state, which is stabilized in the normal mode ϕ, in the basis of local modes.

for more details). We now show that in our case the states in DFS (11) are multimode.

The cat states are encoded in an arbitrary normal mode $k = \phi$. As the normal modes are delocalized over the entire array, the cat states that we discuss here are highly nonlocal. This can be seen explicitly by moving into the basis of local modes

$$|\mathcal{C}^{\pm}\rangle = \mathcal{N}_{\pm}\left(\bigotimes_{j=1}^{N}|\zeta_j\rangle_j \pm \bigotimes_{j=1}^{N}|-\zeta_j\rangle_j\right), \qquad (12)$$

where $\zeta_j = (\zeta/\sqrt{N})e^{-ij\phi}$ [44]. Controlling the phase ϕ (and that of the drive $\theta = 2\phi$), it is possible to prepare different instances of these cat states. In particular, if ϕ is an even multiple of π, Eq. (12) resembles a Greenberger-Horne-Zeilinger (GHZ)-like state, with real and opposite amplitudes; if ϕ is an odd multiple of π, the amplitudes being superimposed are staggered.

These pure states are the multimode version of standard Schrödinger cat states [45]. They have the remarkable property of being both multiphoton and multimode quantum superpositions, and possess genuine multipartite entanglement [21,26,46]. Moreover, such entanglement is of the most useful kind, namely non-Gaussian, which makes Eq. (12) a resource for quantum metrology [2,22,23], quantum information based on continuous variables [20,21,25], and continuous-variable quantum computation [47]. We also stress that the potential of multimode cat states is still largely unexplored. In fact, theoretical studies of multimode cat states has been mostly limited to $N = 2$ (also known as entangled coherent states [21]) due to the current lack of preparation protocols that are at the same time scalable and robust to errors.

To contrast the multimode cat states with standard single-mode cat states, we plot in Figs. 2(b)–2(d) the N-mode Wigner function $W(x_1, \ldots, x_N, p_1, \ldots, p_N)$ of the cat states $|\mathcal{C}^{\pm}\rangle$ stabilized in the normal mode $\phi = 0$ [48]. The unique feature of multimode cat states is the quantum interference in multimode phase space, which manifests itself in interference fringes of the Wigner function in the x_j-x_l plane (for any $j \neq l$) depicted in Figs. 2(c) and 2(d) for $|\mathcal{C}^{+}\rangle$ and $|\mathcal{C}^{-}\rangle$, respectively. This feature is absent for single-mode cat states.

An interesting observation comes from comparing our protocol with known techniques for the generation of multimode cat states in linear optics [2]. In a linear optics network, multimode cat states can be prepared by mixing a *single-mode cat state* $|\mathcal{C}^{\pm}\rangle$ with $N - 1$ vacua. The optics network is represented by a unitary $\hat{T}$ performing the linear transformation $\hat{a}_j = \hat{T}\hat{b}_{2\pi j/N}\hat{T}^{\dagger} = \sum_k T_{jk}\hat{b}_k$ of the input modes $\hat{b}_k$, where $T_{jk} = (1/\sqrt{N})e^{-ijk}$. In our case, as depicted in Fig. 2(e), this linear transformation is automatically implemented by engineering the state of a normal mode. The obvious differences are that our method allows

us to stabilize a cat state in stationary (cavity) modes rather than itinerant modes, and that it does not rely on an external resource (i.e., the input single-mode cat state). Besides that, our strategy possesses yet another fundamental advantage. For a single-mode cat state of amplitude ζ at the input of an interferometer, the corresponding multimode cat state at the output has rescaled local amplitudes $\zeta/\sqrt{N}$; this feature reflects the passive character of the optical network, which does not pump energy into the system. On the other hand, in the driven-dissipative process that we exploit to stabilize the multimode cat state, the total power $\propto NG$ injected into the array increases with the number of resonators N. This in turn allows for the amplitude of the state $|\zeta| \propto \sqrt{N}$ to increase with N. As a result, the multimode cat states can be distributed over an arbitrary number of local modes N with the local amplitudes $|\zeta_j| = |\zeta|/\sqrt{N} = \sqrt{G/U}$ independent of N. This scaling of amplitudes allows for increasing noise bias by using multimode cat states instead of single-mode cat states, which we discuss in detail in Sec. IX.

IV. STEADY-STATE PREPARATION OF MULTIMODE CAT STATES

In the last section we showed that the steady states of Eq. (3) belong to a DFS spanned by multimode cat states. Therefore, depending on the initial state $\hat{\rho}_{\text{in}}$, the state of the array asymptotically converges toward a pure dark state $\alpha|\mathcal{C}^{+}\rangle + \beta|\mathcal{C}^{-}\rangle$ or their incoherent mixtures. Given the unique properties displayed by these cat states [cf. the discussion following Eq. (12)], we now focus on the stabilization of $|\mathcal{C}^{\pm}\rangle$, i.e., we wish to find initial states $\hat{\rho}_{\text{in}}$ for which the array asymptotically approaches these states. At the same time, we should keep in mind that the choice of the initial state $\hat{\rho}_{\text{in}}$ must be experimentally feasible.

In analogy with the preparation of a single-mode even-parity cat state, which can be stabilized starting from the vacuum [9,12], we initialize the array in the N-mode vacuum state $\hat{\rho}_{\text{in}} = |0\rangle\langle 0|$. In Fig. 3 we plot the fidelity c_{++} (c_{--}) of the steady state with the multimode cat state $|\mathcal{C}^{+}\rangle$ ($|\mathcal{C}^{-}\rangle$) as a function of the nonlocal decay rate for different two-photon pump strengths (see Appendix A for more details about the numerical simulations). We can see that c_{++} [blue lines in Fig. 3(a)] is in general smaller than unity and c_{--} [green lines in Fig. 3(b)] is nonzero. Therefore, at variance with the single-mode case, starting from the vacuum does not guarantee reaching the target steady state $|\mathcal{C}^{+}\rangle$. Nonetheless, Fig. 3 provides a clear indication that, for sufficiently strong nonlocal dissipation, fidelities with $|\mathcal{C}^{+}\rangle$ arbitrarily close to unity can be achieved, which renders the preparation of multimode cat states from vacuum feasible in the strong dissipation regime.

The cat state $|\mathcal{C}^{+}\rangle$ can be transformed into a superposition $\cos\alpha|\mathcal{C}^{+}\rangle + i\sin\alpha|\mathcal{C}^{-}\rangle$ of cat states $|\mathcal{C}^{+}\rangle$ and $|\mathcal{C}^{-}\rangle$ by a rotation within the stabilized DFS induced by a weak
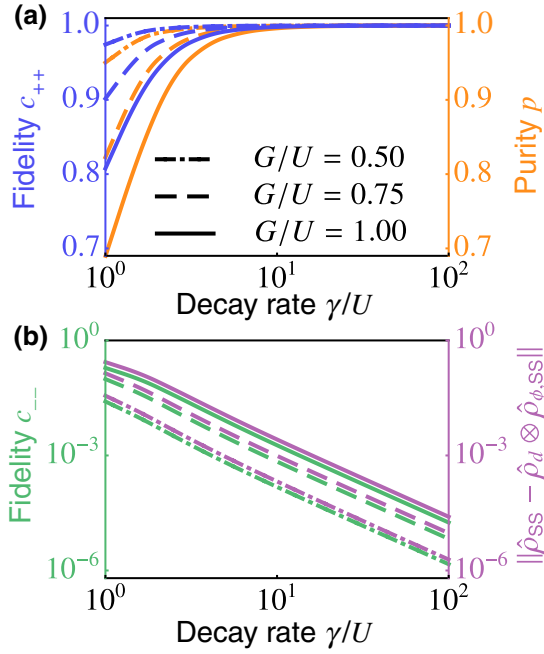
FIG. 3. Steady state for the array initially in the vacuum state. (a) Fidelity c_{++} with $|\mathcal{C}^+\rangle$ (blue lines) and purity p (orange lines) as a function of the decay rate γ for different values of the two-photon pump strength G. (b) Fidelity c_{--} with $|\mathcal{C}^-\rangle$ (green lines) as well as the difference $\|\hat{\rho}_{SS} - \hat{\rho}_d \otimes \hat{\rho}_{\phi,SS}\|$ (purple lines) between the steady state $\hat{\rho}_{SS}$ of the full master equation (3) and the steady state $\hat{\rho}_{\phi,SS}$ of the effective master equation (13) in the Zeno limit as a function of the decay rate γ for different two-photon pump strengths G [identical to panel (a)]. (Here $N = 3$.)

single-photon drive as demonstrated for single-mode cat states [14] (see Appendix C for more details).

The target steady state $|\mathcal{C}^+\rangle$ is not deterministically approached from the initial vacuum for all γ since photon parity is not conserved during the time evolution [49]. The multimode cat states $|\mathcal{C}^\pm\rangle$ spanning the DFS have a well-defined parity as they are ± 1 eigenstates of the generalized parity operator $\hat{\mathcal{P}} = \exp{(i\pi \sum_{j=1}^{N} \hat{a}_j^\dagger \hat{a}_j)}$. However, the photon parity is not a conserved quantity of master equation (3)—a conserved quantity is an operator $\hat{J}$ such that $\mathcal{L}^\dagger \hat{J} = 0$, while $\mathcal{L}^\dagger \hat{\mathcal{P}} = -2 \sum_{k \neq \phi} \gamma_k \hat{b}_k^\dagger \hat{b}_k \hat{\mathcal{P}} \neq 0$, where $\mathcal{L}^\dagger$ is the adjoint Liouvillian [50].

For the initial vacuum, the system starts off in the even-parity subspace, but during the time evolution, it leaks to the odd-parity subspace, leading to nonunit (nonzero) values of the fidelity c_{++} (c_{--}) shown in Fig. 3. For $\gamma \sim G, U$, this leakage leads to a decreased purity p of the steady state [orange lines in Fig. 3(a)], while for sufficiently strong dissipation, the leakage is suppressed and the generalized parity is approximatively conserved (to an arbitrary degree of accuracy). This further confirms that the regime of strong nonlocal dissipation is relevant

for steady-state preparation of the even cat state $|\mathcal{C}^+\rangle$. In this regime, the dynamics at all times can be captured by an effective single-mode theory, as we show in the next section. On the other hand, due to nonconservation of parity and the many-body interaction $\hat{H}_U$, for values of the dissipation rate comparable to the Kerr nonlinearity, we expect the *transient dynamics* to exhibit genuine many-body features.

V. THE ZENO LIMIT

We now have numerical evidence that, in the limit of dominant nonlocal dissipation, the even multimode cat state $|\mathcal{C}^+\rangle$ can be deterministically prepared from the N-mode vacuum. In order to better explain this behavior, in this section we develop an analytical insight into the regime of large nonlocal decay rate γ. For $\gamma \gg G, U$, the many-body interaction $\hat{H}_U$ between normal modes is suppressed: all decaying modes $k \neq \phi$ are strongly damped and only the single normal mode ϕ is populated. Transitions from the vacuum state to excited states of the decaying modes $k \neq \phi$ are inhibited, i.e., they are in the vacuum *at all times*. This is analogous to the quantum Zeno effect [51,52], i.e., the inhibition of quantum transitions due to a frequent projective measurement of a quantum system. In this analogy, the measurement is enacted by the engineered environment via the nonlocal dissipation $\mathcal{L}_\gamma = \sum_k \gamma_k \mathcal{D}[\hat{b}_k]$, which continuously projects all decaying modes onto the vacuum state. In the following, we refer to the limit of a large nonlocal decay rate $\gamma \gg G, U$ as the Zeno limit.

In Appendix B we show that in this limit the reduced density matrix $\hat{\rho}_\phi$ of the nondecaying mode ϕ is described by the effective master equation

$$\dot{\hat{\rho}}_\phi = -i[\hat{H}_\phi, \hat{\rho}_\phi] + \Gamma \mathcal{D}[\hat{b}_\phi^2 - \zeta^2]\hat{\rho}_\phi = \mathcal{L}_\phi \hat{\rho}_\phi, \quad (13)$$

where $\mathcal{L}_\phi$ is the effective single-mode Liouvillian. This effective master equation is derived by treating the Hamiltonian $\hat{H}$ in Eq. (3) as a perturbation to the dominant dissipation $\mathcal{L}_\gamma$ and projecting all decaying modes $k \neq \phi$ onto the vacuum state. Perturbation theory to first order in $\hat{H}$ describes a *unitary Zeno dynamics* governed by the effective Hamiltonian $\hat{H}_\phi = (U/N)(\hat{b}_\phi^{\dagger 2} - \zeta^{*2})(\hat{b}_\phi^2 - \zeta^2)$, namely that of a single-mode KPR [12]. On the other hand, processes that are of second order in $\hat{H}$ lead to an *effective two-photon driven dissipation* term described by the dissipator $\mathcal{D}[\hat{b}_\phi^2 - \zeta^2]$, occurring at a rate $\Gamma = (4U^2/N^2) \sum_{k \neq \phi} 1/\gamma_k$; this effective dissipation is facilitated by virtual excitations of the decaying modes $k \neq \phi$. We thus come to an important conclusion: the emergence of effective two-photon dissipation is the mechanism responsible for the relaxation toward the steady state of the nondecaying mode.

We note that, since it involves second-order processes, dissipation sets in only at long times $t \sim 1/\Gamma \sim \gamma N^2/U^2$. At short times $t \sim N/U$, the mode ϕ undergoes a unitary Zeno dynamics governed by the effective Hamiltonian $\hat{H}_\phi$. A general (model-independent) treatment of the Lindblad master equations with strong dissipation acting on a subset of the degrees of freedom is discussed in detail in Ref. [53], including the derivation of the unitary Zeno dynamics and effective weak dissipation of nondecaying modes.

In Fig. 3(b), we plot the difference $\|\hat{\rho}_{\mathrm{SS}} - \hat{\rho}_d \otimes \hat{\rho}_{\phi,\mathrm{SS}}\|$ (purple lines) between the steady state $\hat{\rho}_{\mathrm{SS}}$ of the full master equation (3) and the steady state $\hat{\rho}_d \otimes \hat{\rho}_{\phi,\mathrm{SS}}$ of the effective master equation (13) as a function of the decay rate γ for different values of G/U, where $\hat{\rho}_d = \bigotimes_{k\neq\phi} |0\rangle_k\langle 0|$ is the $(N-1)$-mode vacuum state and $\|\hat{A}\|^2 = \mathrm{Tr}[\hat{A}^\dagger \hat{A}]$ is the Hilbert-Schmidt norm. We can see that the difference vanishes as $\mathcal{O}(U^2/\gamma^2)$ with increasing decay rate γ. This confirms that, for large enough γ, the effective master equation (13) accurately describes the dynamics of the Kerr-resonator array at long times.

In the Zeno limit, the photon parity $\mathcal{P}_\phi = (-1)^{\hat{b}_\phi^\dagger \hat{b}_\phi}$ is a *conserved quantity* of the effective Liouvillian, i.e., $\mathcal{L}_\phi^\dagger \mathcal{P}_\phi = 0$, as it commutes with both the Hamiltonian $\hat{H}_\phi$ and the jump operator $\hat{b}_\phi^2 - \zeta^2$ [50]. Therefore, in this limit there is no leakage to the odd-parity subspace. This provides a neat explanation for the behavior observed in Fig. 3(a) for large γ and proves that the dissipative dynamics of master equation (3) allows for the steady-state preparation of the even cat state $|\mathcal{C}^+\rangle$ from the vacuum state $|0\rangle$ with a fidelity arbitrarily close to unity.

The rate of convergence toward the steady state is given by the dissipative gap Δ_d, which is determined from the spectrum of the Liouvillian as the smallest nonvanishing real part of the eigenvalues [50]. Since the rate of two-photon dissipation is inversely proportional to the nonlocal decay rate, i.e., $\Gamma \propto \gamma^{-1}$, the dissipative gap $\Delta_d \propto \gamma^{-1}$ retains the same dependence (see Appendix F for more details). For $|\zeta| \gtrsim 1$, the dissipative gap can be approximated as

$$\Delta_d \approx 8\frac{U^2}{N^2}\left(\sum_{k\neq\phi}\frac{1}{\gamma_k}\right)|\zeta|^2 \propto \frac{UG}{N\gamma}. \tag{14}$$

Equation (14) is an important result as it expresses a trade-off between the suppression of the leakage to the odd-parity subspace and the time required to reach the steady-state manifold. The price of an accurate (i.e., near-unit-fidelity) preparation of the even multimode cat state $|\mathcal{C}^+\rangle$ (from the vacuum) is a slow convergence. Although this does not *per se* preclude the stabilization of $|\mathcal{C}^+\rangle$, it becomes problematic in the presence of competing decoherence mechanisms, such as intrinsic photon loss. In Sec. VII, we discuss the impact of this source of decoherence in

the Kerr-resonator array and how it limits the steady-state preparation. Moreover, increasing the number of modes N in the superposition leads to a further increase in the convergence time, which poses a theoretical limit to the scalability of our approach.

VI. ALTERNATIVE MODEL INCLUDING TWO-PHOTON LOSS

To avoid the trade-off between the suppression of the leakage to the odd-parity subspace and the rate of convergence toward the steady state, we consider an alternative model that allows the stabilization of multimode cat states $|\mathcal{C}^\pm\rangle$ while at the same time featuring *a large dissipative gap*. This model is based on an array of dissipatively coupled linear resonators ($U = 0$), subject to local two-photon loss at rate η and two-photon pump with amplitude G, as sketched in Fig. 1(b). The model only requires a small adjustment with respect to our previous model, namely replacing the on-site Kerr nonlinearity with engineered two-photon loss. This alternative model is described by the master equation

$$\dot{\hat{\rho}} = 2\eta \sum_{j=1}^{N} \mathcal{D}\left[a_j^2 - e^{-2ij\phi}\frac{\tilde{\zeta}^2}{N}\right]\hat{\rho} + \sum_k \gamma_k \mathcal{D}[\hat{b}_k]\hat{\rho} = \mathcal{L}\hat{\rho}, \tag{15}$$

where $\tilde{\zeta} = \sqrt{-iNG/\eta}$. The local two-photon driven dissipation described by the term $\mathcal{D}[a_j^2 - e^{-2ij\phi}\tilde{\zeta}^2/N]$ is known to stabilize a DFS whose basis states are even and odd single-mode cat states [9,32]. The local dissipator has been realized experimentally in Refs. [10,14,17].

The dissipatively coupled array of resonators described by master equation (15) exhibits the same DFS as the Kerr-resonator array [see Eq. (11)] with a modified amplitude of the cat states $\zeta \to \tilde{\zeta} = e^{-i3\pi/4}\zeta$ (see Appendix D for a detailed derivation of the DFS). In the Zeno limit of strong nonlocal dissipation $\gamma \gg G, \eta$, the time evolution of mode ϕ is described by an effective master equation

$$\dot{\hat{\rho}}_\phi = 2\frac{\eta}{N}\mathcal{D}[\hat{b}_\phi^2 - \tilde{\zeta}^2]\hat{\rho}_\phi, \tag{16}$$

which is derived by employing first-order perturbation theory where $\mathcal{L}_\eta = 2\eta \sum_{j=1}^{N} \mathcal{D}[a_j^2 - e^{-2ij\phi}\tilde{\zeta}^2/N]$ is treated as a perturbation to the dominant dissipation $\mathcal{L}_\gamma$ (see Appendix E for more details). In comparison to the Kerr-resonator array [cf. Eq. (13)], *the unitary Zeno dynamics is absent* and processes that are of first order in the perturbation $\mathcal{L}_\eta$ give rise to the dissipation $2(\eta/N)\mathcal{D}[b_\phi^2 - \tilde{\zeta}^2]$, leading to convergence toward the DFS. This is in contrast to the Kerr-resonator array, where convergence toward the DFS is due to second-order processes involving virtual excitations of modes $k \neq \phi$.

For this second model, we can completely suppress the leakage to the odd-parity subspace in the Zeno limit (the photon parity $\mathcal{P}_\phi$ is a conserved quantity) and at the same time maintain a large dissipative gap

$$\Delta_d \approx 2\eta|\tilde{\zeta}|^2/N = 2G, \qquad (17)$$

which increases with the strength G of the two-photon drive (see Appendix F for more details). Note that, in contrast to the Kerr-resonator array (14), the dissipative gap Δ_d is independent of γ in the Zeno limit. Importantly, the gap is also independent of system size N, making the preparation of cat states in large arrays feasible.

VII. EFFECTS OF INTRINSIC SINGLE-PHOTON LOSS

In all current circuit QED implementations, unwanted intrinsic photon loss is the dominant source of decoherence, both for the case of the Kerr-resonator array [7,54] and for the model with two-photon driven dissipation [10,14,17]. Photon loss at each resonator is described by the Liouvillian $\mathcal{L}_\kappa \hat{\rho} = \kappa \sum_{j=1}^N \mathcal{D}[\hat{a}_j]\hat{\rho}$. We take intrinsic loss into account by including it in master equation (3), thus obtaining $\dot{\hat{\rho}} = (\mathcal{L} + \mathcal{L}_\kappa)\hat{\rho}$. In contrast to the nonlocal dissipation $\mathcal{L}_\gamma$, which leads to nonuniform dissipation in momentum space, intrinsic photon loss induces uniform dissipation of all normal modes, i.e., $\mathcal{L}_\kappa\hat{\rho} = \kappa \sum_k \mathcal{D}[\hat{b}_k]\hat{\rho}$. For modes $k \neq \phi$, intrinsic photon loss only increases the rate of single-photon dissipation $\gamma_k \rightarrow \gamma_k + \kappa$ that results in their faster decay.

Crucially, intrinsic photon loss gives rise to the single-photon dissipation $\mathcal{D}[\hat{b}_\phi]$ of mode ϕ in addition to the two-photon driven dissipation $\mathcal{D}[\hat{b}_\phi^2 - \zeta^2]$. We remind the reader that the latter is due to local two-photon loss in the model of Sec. VI and arises due to the coupling to modes $k \neq \phi$ in the Kerr-resonator array; see Sec. V. The single-photon dissipation opens a decoherence channel $\hat{b}_\phi|\mathcal{C}^\pm\rangle = \zeta|\mathcal{C}^\mp\rangle$ within DFS (11) at rate $|\zeta|^2\kappa$ [9]. This results in quantum jumps between even and odd cat states, leading to decoherence but not to leakage out of the DFS; even in the presence of single-photon loss, the steady state is confined within the cat manifold. In addition, intrinsic photon loss also causes a decrease in the amplitude $|\zeta|$ of the cat states. However, this decrease is negligible provided that the intrinsic loss rate $\kappa \ll G$ is small (which is the case for state-of-the-art superconducting cavities [54]) as the two-photon drive quickly repumps depleted photons.

Because of the decoherence, the array (for both models) converges at times $t \sim 1/|\zeta|^2\kappa$ toward the fully mixed state $\hat{\rho}_{SS} \approx \frac{1}{2}(|\mathcal{C}^+\rangle\langle\mathcal{C}^+| + |\mathcal{C}^-\rangle\langle\mathcal{C}^-|)$. Therefore, for the deterministic preparation of $|\mathcal{C}^+\rangle$, it is important how the rate of decoherence $|\zeta|^2\kappa$ compares to the rate of convergence toward this state, which corresponds to the dissipative gap Δ_d.

We start by investigating the effects of intrinsic photon loss on the Kerr-resonator array in the Zeno limit, i.e., we consider $\dot{\hat{\rho}}_\phi = -i[\hat{H}_\phi, \hat{\rho}_\phi] + \Gamma\mathcal{D}[\hat{b}_\phi^2 - \zeta^2]\hat{\rho}_\phi + \kappa\mathcal{D}[\hat{b}_\phi]\hat{\rho}_\phi$. We plot the fidelity c_{++} of the instantaneous state $\hat{\rho}_d \otimes \hat{\rho}_\phi(t)$ with the even cat state $|\mathcal{C}^+\rangle$ (blue lines) and the fidelity c_{--} with the odd cat state $|\mathcal{C}^-\rangle$ (green lines) in Fig. 4(a) as a function of time for different values of the intrinsic loss rate κ and starting from the vacuum state. We can see that small intrinsic loss $\kappa/U = 10^{-4}$ is required to reach a large fidelity $c_{++} \approx 0.91$ (blue solid line) before both fidelities c_{++} and c_{--} converge toward the stationary values $c_{++} = c_{--} \approx 0.5$ and the fully mixed state is approached. On the other hand, for a larger loss rate $\kappa/U = 10^{-2}$, the fidelity c_{++} (blue dash-dot line) does not exceed the value $c_{++} = 0.5$ at any time as the rate of decoherence $|\zeta|^2\kappa$ is larger than the rate Δ_d of convergence toward the even cat state. Since the dissipative gap Δ_d (14) is small in the Zeno limit $\gamma \gg G, U$, the steady-state
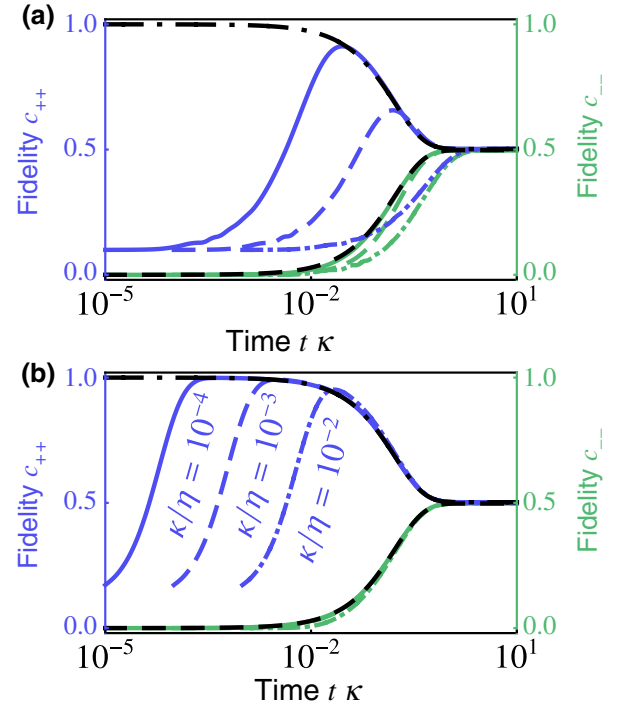

FIG. 4. Dissipative preparation of the even cat state $|\mathcal{C}^+\rangle$ from the vacuum state in the presence of intrinsic photon loss in the Zeno limit. Fidelity of the instantaneous state $\hat{\rho}_d \otimes \hat{\rho}_\phi(t)$ with $|\mathcal{C}^+\rangle$ (blue line) and with $|\mathcal{C}^-\rangle$ (green line) as a function of time t for (a) the Kerr-resonator array and (b) the alternative model with local two-photon loss as well as for intrinsic single-photon loss $\kappa/U = 10^{-4}$ (solid lines), $\kappa/U = 10^{-3}$ (dashed lines), and $\kappa/U = 10^{-2}$ (dash-dot lines). The black dash-dot line and black dashed line show the fidelity c_{++} and the fidelity c_{--}, respectively, for the array initially in the state $|\mathcal{C}^+\rangle$. [Parameters are (a) $N = 3$, $G/U = 1$, and $\gamma/U = 100$, (b) $N = 3$, $G/\eta = 1$. Truncation is at $M_\phi = 20$.]

preparation in the Kerr-resonator array is largely limited by decoherence.

We now consider the impact of photon loss on our second model in the Zeno limit described by the master equation $\dot{\hat{\rho}}_\phi = 2(\eta/N)\mathcal{D}[b_\phi^2 - \tilde{\zeta}^2]\hat{\rho}_\phi + \kappa\mathcal{D}[\hat{b}_\phi]\hat{\rho}_\phi$. From Fig. 4(b) we can see that a large fidelity c_{++} builds up at time orders of magnitude shorter than the characteristic decoherence time $1/\kappa$ ($|\zeta|^2 \sim 1$ here) as the array quickly converges toward the even cat state. The quick convergence is guaranteed by a large dissipative gap Δ_d compared to the decoherence rate $|\zeta|^2\kappa$ with the ratio $|\zeta|^2\kappa/\Delta_d = (N/2)\kappa/\eta$. For all values of the intrinsic loss rate κ, the maximal fidelity is orders of magnitude closer to unity than that for the Kerr-resonator array and is reached at orders-of-magnitude shorter times.

We conclude that local two-photon loss leads to a fast convergence toward the DFS, which allows for an efficient steady-state preparation in the presence of intrinsic photon loss. This is in contrast to the steady-state preparation in the Kerr-resonator array, which is severely limited by decoherence due to slow convergence toward the DFS.

VIII. ROBUSTNESS AGAINST IMPERFECTIONS IN NONLOCAL DISSIPATION

Leveraging strong and tunable nonlocal dissipation plays a crucial role in our preparation protocol, allowing us to select a single nondissipative normal mode and at the same time strongly damping the remaining modes. We now study the robustness of our protocol against imperfections in the nonlocal dissipation, which can appear due to the imperfect tuning of the couplings to the engineered reservoirs.

As the first example of imperfection, we consider a finite accuracy in tuning the phase of the nonlocal dissipators. Imagine we select a plane-wave mode $\phi' \equiv k'$ (whose dissipation we aim to suppress), but due to finite precision, the externally imposed phase $\phi = \phi' + \delta\phi$ of the nonlocal jump operators differs from the target quasimomentum ϕ' by a small offset $\delta\phi$, where we assume that $\delta\phi > 0$ for simplicity. Because of the quasimomentum mismatch $\phi \neq \phi'$, mode ϕ' is no longer a dark mode of the nonlocal dissipator $\mathcal{L}_\gamma$ and, as a consequence, it exhibits nonvanishing single-photon loss at the rate $\gamma_{\phi'} = 2\gamma[1 - \cos(\delta\phi)]$. As discussed in Sec. VII, single-photon loss of the selected mode leads to decoherence within the DFS, which limits the fidelity of prepared cat states. In contrast to the intrinsic photon loss discussed in Sec. VII, which is independent of γ, the single-photon loss rate $\gamma_{\phi'}$ is proportional to γ and it can thus reach significant values in the Zeno limit of large γ. The dependence of the unwanted single-photon loss on γ leads to a trade-off between suppressing the excitations of remaining normal modes in the Zeno limit and keeping the unwanted single-photon loss rate small. As both of these competing processes decrease the fidelity of prepared

cat states, γ has to be optimized to attain efficient cat-state preparation.

We also note that the second smallest single-photon loss rate $\gamma_{\phi'+2\pi/N} = 2\gamma[1 - \cos(2\pi/N - \delta\phi)]$ decreases due to the offset $\delta\phi$. Therefore, in order to achieve strong damping of the remaining normal modes, i.e., $\gamma_{\phi'+2\pi/N} \gg \eta, G$, we not only need a large rate of nonlocal dissipation γ but also a small offset $\delta\phi \ll 2\pi/N$, i.e., the nonlocal phase should be tunable with a sufficiently high resolution. The second condition becomes increasingly challenging for large system sizes N.

So far, we have considered a common offset $\delta\phi$ for all the cavities, so that the overall translational invariance of the model is preserved. We now move to address the effects of disorder. To this end, we consider a general form of imperfections in the engineered nonlocal dissipation $\mathcal{L}_\gamma = \sum_j \gamma_j \mathcal{D}[\hat{a}_j - e^{\phi_j}\hat{a}_{j+1}]$, leading to rates γ_j and phases ϕ_j of jump operators that vary at different bonds between resonators j and $j + 1$. These imperfections break the translational symmetry of the array. As a result, normal modes $\hat{b}_q = \sum_{j=1}^N T_{qj}^*\hat{a}_j$ of the nonlocal dissipator $\mathcal{L}_\gamma$ are no longer plane waves, where T_{jq} is a transformation matrix and $q = 1, 2, \ldots, N$ [55]. As a consequence, pure steady states of master equations (3) and (15) in the form of dark states do not, in general, exist.

However, it is still possible to show that if all but one normal mode $q \neq 1$ experience large single-photon loss $\bar{\gamma}_{q\neq 1}$, cat states can be stabilized and prepared in the selected mode $q = 1$ in the Zeno limit. Here we ordered normal modes q by the loss rate $\bar{\gamma}_q$ from smallest to largest, so that $q = 1$ is now the closest mode to achieve the ideal nondissipative condition. For concreteness, we focus here on the alternative model (15) with local two-photon loss and with a vanishing two-photon pump phase $\theta = 0$ [56]. In the Zeno limit $\bar{\gamma}_{q\neq 1} \gg \eta, G, \bar{\gamma}_1$, the time evolution of mode $q = 1$ is described by an effective master equation

$$\dot{\hat{\rho}}_1 = 2\frac{\bar{\eta}}{N}\mathcal{D}[\hat{b}_1^2 - \bar{\zeta}^2]\hat{\rho}_1 + \bar{\gamma}_1\mathcal{D}[\hat{b}_1]\hat{\rho}_1, \qquad (18)$$

where $\bar{\eta} = \eta N \sum_{j=1}^N |T_{j1}|^4$, $\bar{G} = G \sum_{j=1}^N T_{j1}^{*2}$, and $\bar{\zeta} = \sqrt{-iN\bar{G}/\bar{\eta}}$ (see Appendix G for more details). Despite the broken translational invariance, we still recover two-photon driven dissipation at rate $\bar{\eta}$, which stabilizes a DFS spanned by cat states with amplitudes $\bar{\zeta}$. We then reach a remarkable conclusion: in the Zeno limit, disorder affects only quantitatively the nature of two-photon driven dissipation, leading to a modified amplitude of cat states $\bar{\zeta} = \sqrt{-iN\bar{G}/\bar{\eta}}$ and of the dissipative gap $\Delta_d \approx 2|\bar{G}|$. This provides analytical insight into the robustness of the Zeno limit to disorder. However, from Eq. (18) we also see a qualitative change with respect to the disorderless case (16), namely the appearance of an additive single-photon loss term. Because of imperfections, nonlocal dissipation can give rise to single-photon loss of the

selected mode $q = 1$. In particular, for a nontrivial over-all phase $\Phi = \sum_{j=1}^{N} \phi_j \neq 2n\pi$, where n is any integer, the dark mode condition, $T_{(j+1)1} = e^{\phi_j} T_{j1}$ for all j, is not compatible with periodic boundary conditions and, as a consequence, the selected mode exhibits a nonvanishing single-photon loss rate $\bar{\gamma}_1 \neq 0$.

We now consider disorder in nonlocal dissipation rates $\gamma_j = \gamma(1 + \sigma \delta\gamma_j)$ and jump-operator phases $\phi_j = (\pi/3)\sigma\delta\phi_j$, where $\delta\gamma_j$ and $\delta\phi_j$ are normally distributed random variables and σ is the strength of disorder. The cat-state amplitude $\bar{\zeta}$ and the dissipative gap Δ_d are only marginally modified in the presence of moderate disorder $\sigma \lesssim 0.25$ (see Appendix G for more details). On the other hand, the single-photon loss rate can reach considerable values even for moderate disorder, leading to significant decoherence within the DFS and, as a result, to a decreased fidelity of prepared cat states. The fidelity of the prepared state is determined by the ratio of the decoherence rate $|\bar{\zeta}|^2\bar{\gamma}_1$ and the dissipative gap Δ_d; see Sec. VII. We plot the distribution of the ratio in a disordered array as a function of the disorder strength in Fig. 5(a). We can see that, with increasing disorder strength, it is more likely to obtain a decoherence rate $|\bar{\zeta}|^2\bar{\gamma}_1 \sim \Delta_d$ comparable to the dissipative gap Δ_d, which severely limits the fidelity of prepared
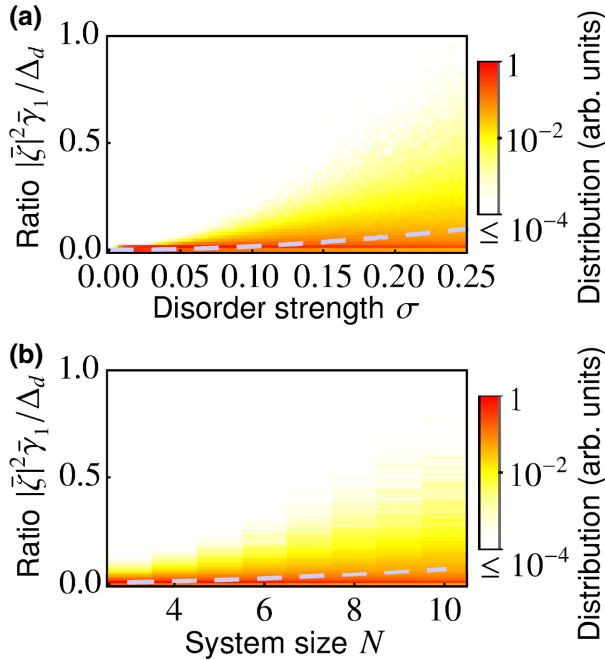

(a)

(b)

FIG. 5.   Effects of disorder in nonlocal dissipation in the alternative model. Distribution (color gradient) of the ratio between the rate of decoherence $|\bar{\zeta}|^2\bar{\gamma}_1$ and the dissipative gap Δ_d for disorder in nonlocal decay rates γ_j and jump-operator phases ϕ_j as a function of (a) the disorder strength σ and (b) system size N. Blue dashed lines show the average value of the ratio. [Parameters are (a) $N = 3$, $\gamma/\eta = 3$, $G/\eta = 1$, (b) $\sigma = 0.075$, $\gamma/\eta = 4.5/[1 - \cos(2\pi/N)]$, $G/\eta = 1$.]

cat states. On the other hand, the decoherence rate $|\bar{\zeta}|^2\bar{\gamma}_1$ remains, on average (blue dashed line), an order of magnitude smaller than the dissipative gap Δ_d even for moderate disorder $\sigma \sim 0.25$, allowing the preparation of cat states with a large fidelity.

We now study the effects of disorder in arrays with increasing system size N. In order to keep the smallest loss rate of the remaining modes $\bar{\gamma}_2 \approx \gamma'$ approximately constant with increasing system size, we increase the non-local dissipation rate $\gamma = \gamma'/2[1 - \cos(2\pi/N)]$. We plot the distribution of the ratio between the decoherence rate $|\bar{\zeta}|^2\bar{\gamma}_1$ and the dissipative gap Δ_d for a constant disorder strength $\sigma = 0.075$ as a function of system size N in Fig. 5(b). We can see that, with increasing system size, the ratio increases on average (blue dashed line) and it is more likely to obtain a decoherence rate $|\bar{\zeta}|^2\bar{\gamma}_1 \sim \Delta_d$ comparable to the dissipative gap Δ_d. The decoherence rate $|\bar{\zeta}|^2\bar{\gamma}_1 \propto N$ increases due to the increasing cat-state amplitude $|\bar{\zeta}| \propto \sqrt{N}$ while the single-photon loss rate $\bar{\gamma}_1$ and the dissipative gap Δ_d stay approximately constant with increasing system size (see Appendix G).

We note that, for some disorder realizations, the over-all phase Φ is vanishingly small and, as a consequence, the single-photon loss rate $\bar{\gamma}_1$ is negligible. For these disorder realizations, the dominant source of decoherence within the DFS is single-photon amplification $\mathcal{D}[\hat{b}_1^\dagger]$. Single-photon amplification is a second-order perturbation process in the two-photon pump $\hat{H}_G$ and it is facilitated by virtual excitations of strongly decaying normal modes $q \neq 1$. However, single-photon amplification does not severely limit the fidelity of prepared cat states since it is suppressed in the Zeno limit as its rate is inversely proportional to γ (see Appendix H for more details).

In conclusion, due to imperfections in nonlocal dissipation, the selected normal mode is not a dark mode of the nonlocal dissipator. Remarkably, cat states can still be stabilized and prepared in the selected mode in the Zeno limit, albeit with decreased fidelity as decoherence due to unwanted single-photon loss sets in. Since the single-photon loss rate is proportional to the nonlocal dissipation rate γ, we face a trade-off between suppressing the excitations of remaining normal modes and keeping the decoherence rate small. The effects of decoherence are more pronounced for large system sizes due to the increasing cat-state amplitude. However, we can conclude that, for moderate disorder strengths and moderate system sizes, the decoherence rate remains, on average, an order of magnitude smaller that the dissipative gap, thus allowing for the preparation of cat states with a large fidelity even in the presence of imperfections.

IX. NOISE BIAS OF MULTIMODE CAT STATES

A manifold spanned by Schrödinger cat states is advantageous for encoding and protecting quantum information

because it experiences biased noise [9], which means that states in the manifold display an asymmetric response to different kinds of noise channels. This can considerably simplify the quantum-error-correcting protocols required to protect quantum information from decoherence. In this section we first recall the most important features of biased noise and then show that multimode cat states offer an enhanced noise bias over the single-mode cat states considered so far.

For concreteness, let us assume that we encode the logical quantum states into the superposition of single-mode cat states $|0/1\rangle_L \equiv (|\mathcal{C}^+\rangle \pm |\mathcal{C}^-\rangle)/\sqrt{2} \approx |\pm\zeta\rangle$ (the last approximation is excellent for $|\zeta| \gtrsim 2$) as, for instance, realized with a single KPR cat state of amplitude $\zeta = i\sqrt{G/U}$ [12]. The overlap between the coherent states $|\langle+\zeta|-\zeta\rangle| = \exp(-2|\zeta|^2)$ is exponentially suppressed with the number of photons $|\zeta|^2$. This simple fact endows the encoding with a natural protection against noise. Indeed, by increasing the amplitude, the coherent states move further apart and it becomes extremely unlikely for any noise process to cause a jump between $|0\rangle_L$ and $|1\rangle_L$, i.e., to generate a so-called bit-flip error. Note that increasing the amplitude comes at the price of an increased phase-flip error rate, i.e., noise-induced flips between $|\pm\rangle_L \equiv |\mathcal{C}^\pm\rangle$ eigenstates. However, it can be shown that the phase-flip error rate increases only linearly with respect to the number of photons in the mode. As a result, there is a net bias $\exp(-2|\zeta|^2)/|\zeta|^2$ between the error rates experienced by a single resonator [9]. Such noise bias has recently been experimentally observed and tuned in Ref. [17].

Let us now consider a similar encoding, but replacing the single-mode cat states with multimode cat states $|\mathcal{C}^\pm\rangle_\phi$. This choice allows for a further exponential improvement in the noise bias, achieving $\exp(-2N|\zeta|^2)/(N|\zeta|^2)$; the expression is written in terms of the single-mode amplitude, for instance for the case of Kerr nonlinearity $\zeta_{N\text{-mode}} \equiv i\sqrt{NG/U} = \sqrt{N}\zeta$. The bias exponentially increases with respect to both the number of coherent photons in each resonator (set by the ratio between the two-photon pump and either the Kerr nonlinearity or the two-photon loss rate) and the number of resonators in the array. While the first feature leads to "standard noise bias" and is already exploited for qubit encoding in a single-mode cat manifold, the second feature is unique to our model. The physical reason for this is that the total number of photons in the multimode cat state stabilized in the resonator array increases with the number of resonators, as discussed in Sec. III. Therefore, the multimode DFS (11) can encode a qubit with bit-flip errors exponentially suppressed with system size N, gaining an exponential improvement in the noise bias compared to single-mode cat states. This can be exploited to realize a *protected quantum memory* that only suffers from phase-flip errors, which can in turn be corrected by simple classical error-correction techniques (e.g., a simple repetition code) [15].

X. EXPERIMENTAL PARAMETERS

For both models of cat-state preparation, the regime $\gamma \gg G, U, \eta \gg \kappa$ is required to suppress excitations of remaining normal modes ($\gamma \gg G, U, \eta$, as discussed in Sec. V) while at the same time reducing the effects of decoherence due to intrinsic single-photon loss ($U, \eta \gg \kappa$, as discussed in Sec. VII). Strong Kerr nonlinearities can be effectively induced both in three-dimensional microwave cavities [54] and on-chip resonators [42], via coupling to a Josephson junction, resulting in photon-photon interactions far exceeding the photon loss rate. The induced Kerr nonlinearity $U \sim 100$–$1000\,$kHz can be larger than intrinsic loss rates $\kappa \sim 10$–$100\,$Hz of state-of-the-art three-dimensional cavities [57,58] by orders of magnitude, with feasible ratios $\kappa/U \sim 10^{-5} - 10^{-3}$. The stabilization of Schrödinger cat states in a single Kerr resonator using a parametric two-photon drive has been demonstrated by Grimm *et al.* [7], who reported an amplitude $|\zeta| \sim 1$, which corresponds to $G/U \sim 1$. In an array, the amplitude $|\zeta| \propto \sqrt{N}$ of the cat states increases with the number of Kerr resonators. Local two-photon loss can be realized in a similar three-dimensional circuit QED architecture [9] at rate $\eta \sim 100\,$kHz [10] with a feasible ratio $\kappa/\eta = 10^{-2}$ [14]. It has been employed for the stabilization of a single-mode Schrödinger cat state with an amplitude $|\zeta| \sim 1$ [10].

In addition to coupling neighboring resonators to a transmission line as discussed in Ref.[31], nonlocal dissipation can also be implemented by coupling to a strongly decaying microwave mode with a feasible decay rate $\kappa_A \sim 100\,$MHz [10]. Microwave modes can be coupled using parametrically driven elements consisting of several Josephson junctions reaching coupling strengths $g \sim 100\,$MHz, as demonstrated in planar superconducting circuits [59,60]. Using a weaker parametric drive such that $g \ll \kappa_A$, one can achieve effective nonlocal dissipation at rate $\gamma \sim g^2/\kappa_A$ by adiabatically eliminating the strongly decaying mode. It is also feasible to achieve the Zeno limit of strong nonlocal dissipation $\gamma \gg G, U, \eta$ as the parametric coupling g and the decay rate κ_A can be sufficiently large.

Finally, we stress that, while multimode cat states can be stabilized and prepared in resonator arrays with a large system size N, all characteristic features of the multimode cat-state preparation discussed in this manuscript—and especially the exponentially enhanced noise bias—can already be observed for a small system size $N = 3$.

XI. CONCLUSIONS

We showed that a two-dimensional manifold spanned by superpositions of multimode Schrödinger cat states can be stabilized in an array of resonators coupled via nonlocal dissipation. The required nonlinearity, which is either of the Kerr type or an engineered two-photon loss, acts

locally on each resonator while the dissipative coupling is linear, which makes our proposal particularly convenient for experimental implementations. The two models we put forward are readily realizable with state-of-the-art circuit QED architectures.

In the Zeno limit of strong nonlocal dissipation, we showed that the even-parity multimode cat state can be prepared from the initial vacuum state with a fidelity approaching unity. In the Kerr-resonator array, the steady-state preparation is limited by decoherence due to intrinsic photon loss, which sets in at long times, as the relaxation toward the steady state is due to a weak effective two-photon dissipation, resulting in a slow rate of convergence. On the other hand, local two-photon loss gives rise to a quick convergence toward the multimode cat states, allowing for their efficient preparation. Multimode cat states can be stabilized and prepared in the Zeno limit even in the presence of imperfections in nonlocal dissipation, albeit with decreased fidelity as an additional decoherence channel sets in. Importantly, the rate of convergence toward the cat states is independent of system size, making the steady-state preparation scalable. Scaling toward large system sizes requires a good suppression of imperfections in nonlocal dissipation as they lead to decoherence that is more pronounced in large systems. Our protocol exploits N local two-photon pumps, allowing for the amplitude $|\zeta| \propto \sqrt{N}$ of the multimode cat states to increase with the number of resonators in the array N. This in turn leads to an exponentially increasing noise bias of the cat manifold, which can be exploited for the implementation of a quantum memory with enhanced protection.

Being able to prepare multimode cat states in a deterministic, robust, and scalable fashion is of direct relevance for applications in quantum metrology, quantum computation, and quantum information. In quantum computation, especially in the context of bosonic codes based on cat qubits, multimode cat states correspond to GHZ states, which are a required resource for universal fault-tolerant quantum computing, e.g., by enabling Toffoli state preparation [6]. In quantum metrology, multimode cat states can provide a source of non-Gaussian multimode light needed for attaining Heisenberg scaling [22,23]; they are also a source of non-Gaussian multipartite entanglement to generate non-Gaussian cluster states [61]. Moreover, our proposal may also foster multimode extensions of existing protocols currently limited by the lack of non-Gaussian resources beyond the single- or two-mode case. Multimode cat states are also relevant to fundamental aspects of quantum theory, e.g., to test predictions of decoherence theory and explore the quantum-to-classical transition [62].

Our treatment of dissipatively coupled cavity arrays opens new avenues in quantum reservoir engineering [30] as it allows for tailored dissipation in momentum space. Interesting future directions are the stabilization of other

non-Gaussian multimode entangled states using different on-site models, reservoir engineering with multiple normal modes with different quasimomenta by employing different nonlocal reservoirs, and tailoring dissipation in momentum space of higher dimensions. Finally, for the specific models considered in this work, even though the steady states can be described analytically for any system parameters and the transient dynamics can be well described in the Zeno limit by an effective master equation for a single normal mode, much less has been understood about the driven-dissipative many-body dynamics for the nonlocal dissipation rate comparable to the Kerr nonlinearity, which will be subject of a future investigation.

Note added.—Recently, two related papers have been published: one that investigates mixed steady states of dissipatively coupled Kerr-resonator arrays, which correspond to the ground states of a frustrated antiferromagnet [63]; and another that studies the generation and detection of two-mode cat states in dissipatively coupled parametric oscillators [64] for the particular case $N = 2$ only.

APPENDIX A: NUMERICAL SIMULATIONS OF MASTER EQUATION (3)

In this appendix we provide details about numerical simulations of master equation (3) and its conserved quantities.

In general, steady states that are neither dark states nor their incoherent mixtures can exist [40]. However, we verified that master equation (3) has no steady states lying outside of DFS (11) by numerically solving for $\mathcal{L}\hat{\rho}_{SS} = 0$ for $N = 3, 4$ and various values of the nonlocal decay rate γ/U and two-photon drive strength G/U. We truncate the infinitely dimensional Hilbert space considering only M_k lowest-energy levels of each mode k.

Each coefficient $c_\mu = \text{Tr}[\hat{\rho}_{in}\hat{J}_\mu]$ of DFS (11) is associated with a conserved quantity $\hat{J}_\mu$ and encodes the information about $\hat{\rho}_{in}$ that is preserved during the time evolution. As a result, conserved quantities can be used to find the particular steady state for a given initial state. Conserved quantities $\hat{J}_\mu$ are formally defined as solutions of

$\mathcal{L}^{\dagger}\hat{J}_{\mu} = 0$, where $\mathcal{L}^{\dagger}$ is the adjoint Liouvillian and

$$\mathcal{L}^{\dagger}\hat{J}_{\mu} = i[\hat{H}, \hat{J}_{\mu}] + \sum_{k \neq \phi} \gamma_k \left[\hat{b}_k^{\dagger} \hat{J}_{\mu} \hat{b}_k - \frac{1}{2}\{\hat{J}_{\mu}, \hat{b}_k^{\dagger}\hat{b}_k\} \right],$$
(A1)

and $\{\cdot, \cdot\}$ is the anticommutator [50]. We solve numerically for the conserved quantities. Finding conserved quantities, which are biorthogonal to the basis operators $\hat{\xi}_{\pm\pm} = |\mathcal{C}^{\pm}\rangle\langle\mathcal{C}^{\pm}|$ of the DFS, i.e., $\mathrm{Tr}[\hat{J}_{\mu}^{\dagger}\hat{\xi}_{\beta}] = D_{\mu}\delta_{\mu\beta}$, we can determine coefficients $c_{\mu} = \mathrm{Tr}[\hat{J}_{\mu}^{\dagger}\hat{\rho}_{\mathrm{in}}]$ of the particular steady state for a given initial state $\hat{\rho}_{\mathrm{in}}$. Normalization $D_{\mu} = 1$ for all μ guarantees that $\hat{\rho}$ is a density matrix. We plotted in Fig. 3 in the main text the fidelities with the even cat state and the odd cat state as well as the purity of the particular steady state for the initial vacuum state, where we used the following truncation of the Hilbert space: $M_{k=\phi} = 12$ and $M_{k\neq\phi} = 3$ for $G/U = 0.5$, $M_{k=\phi} = 16$ and $M_{k\neq\phi} = 3$ for $G/U = 0.75$, and $M_{k=\phi} = 18$ and $M_{k\neq\phi} = 3$ for $G/U = 1$.

APPENDIX B: EFFECTIVE MASTER EQUATION IN THE ZENO LIMIT

In this appendix, we describe the effective Zeno dynamics of mode $k = \phi$ in the regime of strong nonlocal dissipation, which acts as a continuous measurement projecting all modes $k \neq \phi$ onto the vacuum state. We derive an effective master equation for mode ϕ employing the Dyson series of the Liouvillian dynamics, which was described in detail in Ref. [53].

We start by rescaling time $\tau = \gamma t$ in master equation (3), obtaining

$$\frac{\partial \hat{\rho}(\tau)}{\partial \tau} = \sum_{k \neq \phi} \frac{\gamma_k}{\gamma} \mathcal{D}[\hat{b}_k]\hat{\rho}(\tau) - \frac{i}{\gamma}[\hat{H}, \hat{\rho}(\tau)]$$
$$= (\bar{\mathcal{L}}_d + \mathcal{K})\hat{\rho}(\tau),$$
(B1)

where $\bar{\mathcal{L}}_d = \sum_{k\neq\phi}(\gamma_k/\gamma)\mathcal{D}[\hat{b}_k]$ and $\mathcal{K} = -(i/\gamma)[\hat{H}, \cdot]$. In the limit of strong dissipation $\gamma_k \gg U, G$, for all $k \neq \phi$, we can treat $\mathcal{K}$ as a perturbative term. A general solution of Eq. (B1) can be written as

$$\hat{\rho}(\tau) = \mathcal{U}(\tau)\rho(0),$$
(B2)

where $\mathcal{U}(\tau)$ is the propagator satisfying

$$\mathcal{U}(\tau) = e^{\bar{\mathcal{L}}_d\tau}\left(1 + \int_0^{\tau} ds\, e^{-\bar{\mathcal{L}}_d s}\mathcal{K}\mathcal{U}(s)\right).$$
(B3)

By iterating this equation, we obtain the Dyson series for the propagator

$$\mathcal{U}(\tau) = e^{\bar{\mathcal{L}}_d\tau}\left(1 + \int_0^{\tau} d\tau_1\, e^{-\bar{\mathcal{L}}_d\tau_1}\mathcal{K}\, e^{\bar{\mathcal{L}}_d\tau_1}\right.$$
$$+ \int_0^{\tau} d\tau_1\, e^{-\bar{\mathcal{L}}_d\tau_1}\mathcal{K}\, e^{\bar{\mathcal{L}}_d\tau_1}$$
$$\left. \times \int_0^{\tau_1} d\tau_2\, e^{-\bar{\mathcal{L}}_d\tau_2}\mathcal{K}\, e^{\bar{\mathcal{L}}_d\tau_2} + \cdots\right),$$
(B4)

where the ellipsis denotes terms of third and higher orders in $\mathcal{K}$.

Mode ϕ does not experience any dissipation $(\mathrm{Tr}_d\bar{\mathcal{L}}_d)\hat{\rho}_{\phi} = \hat{\rho}_{\phi}$, where $\hat{\rho}_{\phi} = \mathrm{Tr}_d\hat{\rho}$ is the reduced density matrix of mode ϕ and Tr_d denotes the trace over all decaying modes $k \neq \phi$. The dissipator $\bar{\mathcal{L}}_d$ targets a unique state $\hat{\rho}_d$ in the reduced Hilbert space of all decaying modes $k \neq \phi$, i.e.,

$$(\mathrm{Tr}_{\phi}\bar{\mathcal{L}}_d)\hat{\rho}_d = 0,$$
(B5)

where Tr_{ϕ} is the trace over mode ϕ. The unique steady state is the vacuum state $\hat{\rho}_d = \bigotimes_{k\neq\phi}|0\rangle_k\langle 0|$. The projection onto the kernel of $\bar{\mathcal{L}}_d$ is $\mathcal{P}_d = \lim_{\tau\to\infty}\exp(\bar{\mathcal{L}}_d\tau)$ and obeys the relations

$$\bar{\mathcal{L}}_d\mathcal{P}_d = \mathcal{P}_d\bar{\mathcal{L}}_d = \mathcal{P}_d$$
(B6)

and

$$\mathcal{P}_d\hat{X} = \hat{\rho}_d \otimes \mathrm{Tr}_d\hat{X}$$
(B7)

for an arbitrary density matrix or operator $\hat{X}$.

For strong dissipation $\gamma_k \gg U, G$, the dynamics of the system is constrained to the dissipation-free subspace $\hat{\rho}(\tau) = \hat{\rho}_d \otimes \hat{\rho}_{\phi}(\tau)$ at all times $\tau \gg 1$ [53]. The dynamics of the reduced density matrix $\hat{\rho}_{\phi}(\tau)$ is described by the propagator $\mathcal{P}_d\mathcal{U}(\tau)\mathcal{P}_d$. Writing the Dyson series for the propagator up to the second order in $\mathcal{K}$, we obtain

$$\mathcal{P}_d\mathcal{U}(\tau)\mathcal{P}_d = \mathcal{P}_d + \tau\mathcal{P}_d\mathcal{K}\mathcal{P}_d + \mathcal{P}_d\mathcal{K}\int_0^{\tau} d\tau_1$$
$$\times \int_0^{\tau_1} d\tau_2\, e^{\bar{\mathcal{L}}_d(\tau_1-\tau_2)}\mathcal{K}\mathcal{P}_d + \mathcal{O}\left(\frac{U^3}{\gamma^3}\right),$$
(B8)

where we have used Eq. (B6). We explicitly evaluate the second-order term in the Dyson series in the Supplemental Material to obtain [65]

$$\mathcal{P}_d\mathcal{U}(\tau)\mathcal{P}_d = \mathcal{P}_d + \tau\mathcal{P}_d\mathcal{K}\mathcal{P}_d + \frac{\tau^2}{2}(\mathcal{P}_d\mathcal{K}\mathcal{P}_d)^2$$
$$+ \tau\frac{\Gamma}{\gamma}\mathcal{D}[\hat{b}_{\phi}^2 - \zeta^2]\mathcal{P}_d + \mathcal{O}\left(\frac{U^3}{\gamma^3}\right).$$
(B9)

We now consider that we initially start with a state in the dissipation-free subspace, i.e., $\hat{\rho}(0) = \hat{\rho}_d \otimes \hat{\rho}_{\phi}(0)$.

The time evolution within the dissipation-free subspace is described by $\hat{\rho}_\phi(\tau) = \text{Tr}_d\{\mathcal{P}_d\mathcal{U}(\tau)\mathcal{P}_d[\hat{\rho}_d \otimes \hat{\rho}_\phi(0)]\}$. To obtain a master equation in a differential form, we use the equivalence $\partial\hat{\rho}_\phi/\partial\tau = \lim_{\tau\to 0}\{\hat{\rho}_\phi(\tau) - \hat{\rho}_\phi(0)\}/\tau$. Using the Dyson series (B9) and rescaling back time, $t = \tau/\gamma$, we obtain the effective master equation (13) in Lindblad form. The effective Hamiltonian $\hat{H}_\phi = \text{Tr}_d[(\hat{\rho}_d \otimes \hat{I}_\phi)\hat{H}]$ is the projection of the full Hamiltonian $\hat{H}$ onto the dissipation-free subspace, where $\hat{I}_\phi$ is the identity operator in the reduced Hilbert space of mode ϕ.

APPENDIX C: ROTATION WITHIN THE STABILIZED DFS

We consider a weak single-photon drive $\hat{H}_\lambda = \lambda(e^{ij\phi}\hat{a}_j + e^{-ij\phi}\hat{a}_j^\dagger)$ applied to an arbitrary single resonator j. In the Zeno limit $\gamma \gg U, G, \lambda$, the dynamics of mode ϕ is described by the effective master equation

$$\dot{\hat{\rho}}_\phi = -i[\hat{H}_\phi + \hat{H}_{\phi,\lambda}, \hat{\rho}_\phi] + \Gamma\mathcal{D}[\hat{b}_\phi^2 - \zeta^2]\hat{\rho}_\phi. \quad (C1)$$

To derive the effective master equation, we followed the same steps as in Appendix B for the Kerr-resonator array without the single-photon drive. The single-photon drive $\hat{H}_\lambda$ of resonator j gives rise to the single-photon drive $\hat{H}_{\phi,\lambda} = (\lambda/\sqrt{N})(\hat{b}_\phi + \hat{b}_\phi^\dagger)$ of mode ϕ, which is a first-order process in $\hat{H}_\lambda$. Note that the single-photon drive $\hat{H}_\lambda$ in combination with the Kerr nonlinearity $\hat{H}_U$ and the two-photon drive $\hat{H}_G$ does not lead to any second-order effect due to the strong suppression of exactions of decaying modes and the conservation of total quasimomentum.

It has been shown in Ref. [9] that the single-photon drive $\hat{H}_{\phi,\lambda}$ induces the rotation

$$\hat{R}(\alpha) = \cos\alpha(|\mathcal{C}^+\rangle\langle\mathcal{C}^+| + |\mathcal{C}^-\rangle\langle\mathcal{C}^-|)$$
$$+ i\sin\alpha(|\mathcal{C}^+\rangle\langle\mathcal{C}^-| + |\mathcal{C}^-\rangle\langle\mathcal{C}^+|) \quad (C2)$$

within the DFS stabilized by two-photon driven dissipation $\mathcal{D}[\hat{b}_\phi^2 - \zeta^2]$, provided that the drive strength $\lambda/\sqrt{N}$ is small compared to the rate Γ of two-photon driven dissipation. The even cat state $|\mathcal{C}^+\rangle$, which is dissipatively prepared from the initial vacuum state, can be transformed into a superposition $\hat{R}(\alpha)|\mathcal{C}^+\rangle = \cos\alpha|\mathcal{C}^+\rangle + i\sin\alpha|\mathcal{C}^-\rangle$ of cat states $|\mathcal{C}^+\rangle$ and $|\mathcal{C}^-\rangle$ by the rotation $\hat{R}(\alpha)$.

APPENDIX D: DECOHERENCE-FREE SUBSPACE OF THE ALTERNATIVE MODEL (15)

In this appendix, we discuss the steady states of the alternative model with local two-photon loss described by master equation (15).

We start by writing the dissipator

$$2\eta\sum_{j=1}^N \mathcal{D}\left[\hat{a}_j^2 - e^{-2ij\phi}\frac{\tilde{\zeta}^2}{N}\right] = -i(\hat{H}_{\text{eff}}\hat{\rho} - \hat{\rho}\hat{H}_{\text{eff}}^\dagger) + \mathcal{J}\hat{\rho} \quad (D1)$$

in a form of the non-Hermitian Hamiltonian $\hat{H}_{\text{eff}}$ and the jump term $\mathcal{J}\hat{\rho}$ that can be expressed in the plane-wave basis as

$$\hat{H}_{\text{eff}} = -i\frac{\eta}{N}\sum_{k_1,k_2,k_3,k_4}\delta_{k_1+k_2,k_3+k_4}(\hat{b}_{k_1}^\dagger\hat{b}_{k_2}^\dagger - \delta_{k_1\phi}\delta_{k_2\phi}\zeta^{*2})$$
$$\times (\hat{b}_{k_3}\hat{b}_{k_4} - \delta_{k_3\phi}\delta_{k_4\phi}\tilde{\zeta}^2), \quad (D2)$$
$$\mathcal{J}\hat{\rho} = 2\frac{\eta}{N}\sum_{k_1,k_2,k_3,k_4}\delta_{k_1+k_2,k_3+k_4}(b_{k_1}b_{k_2} - \delta_{k_1\phi}\delta_{k_2\phi}\tilde{\zeta}^2)$$
$$\times \hat{\rho}(\hat{b}_{k_3}^\dagger\hat{b}_{k_4}^\dagger - \delta_{k_3\phi}\delta_{k_4\phi}\tilde{\zeta}^{*2}), \quad (D3)$$

where the arguments $k_1 + k_2$ and $k_3 + k_4$ are defined modulo 2π. Similarly to the Kerr-resonator array, we look for pure steady states $\hat{\rho}_{\text{SS}} = |\Psi\rangle\langle\Psi|$ with all modes $k \neq \phi$ being in the vacuum state, in which case the nonlocal dissipators $\sum_k \gamma_k\mathcal{D}[\hat{b}_k]\hat{\rho}_{\text{SS}} = 0$ in Eq. (15) vanish. Using $\hat{b}_k\hat{\rho}_{\text{SS}} = \hat{\rho}_{\text{SS}}\hat{b}_k^\dagger = 0$ for all $k \neq \phi$, we evaluate all remaining terms in master equation (15), obtaining $\hat{H}_{\text{eff}}\hat{\rho}_{\text{SS}} = -i(\eta/N)\sum_k(\hat{b}_k^\dagger\hat{b}_{2\phi-k}^\dagger - \delta_{k\phi}\tilde{\zeta}^{*2})(\hat{b}_\phi^2 - \tilde{\zeta}^2)\hat{\rho}_{\text{SS}}$, $\hat{\rho}_{\text{SS}}\hat{H}_{\text{eff}}^\dagger = i(\eta/N)\sum_k\hat{\rho}_{\text{SS}}(\hat{b}_\phi^{\dagger 2} - \tilde{\zeta}^{*2})(\hat{b}_k\hat{b}_{2\phi-k} - \delta_{k\phi}\tilde{\zeta}^2)$, and $\mathcal{J}\hat{\rho}_{\text{SS}} = 2(\eta/N)(\hat{b}_\phi^2 - \tilde{\zeta}^2)\hat{\rho}_{\text{SS}}(\hat{b}_\phi^{\dagger 2} - \tilde{\zeta}^{*2})$. All three remaining terms vanish if the pure steady state is one of the coherent states $\hat{b}_\phi|\psi\rangle = \hat{b}_\phi| \pm \tilde{\zeta}\rangle = \pm\tilde{\zeta}|\tilde{\zeta}\rangle$ or an arbitrary superposition of these coherent states. We conclude that an arbitrary superposition of coherent states $| \pm \tilde{\zeta}\rangle$ is a steady state of the master equation satisfying $\mathcal{L}\hat{\rho}_{\text{SS}} = 0$. Similarly as for the array of Kerr resonators, all possible superpositions of coherent states $| \pm \tilde{\zeta}\rangle$ and their incoherent admixtures form DFS (11). We numerically confirm that there are no steady states lying outside DFS (11).

APPENDIX E: EFFECTIVE MASTER EQUATION IN THE ZENO LIMIT FOR THE ALTERNATIVE MODEL (15)

In this appendix, we derive the effective master equation for mode ϕ for the alternative model (15) with local two-photon loss in the Zeno limit of strong nonlocal dissipation. We follow the same steps in the derivation as for the Kerr-resonator array in Appendix B.

We start by rescaling time $\tau = \gamma t$ in master equation (15), obtaining

$$\frac{\partial \hat{\rho}(\tau)}{\partial \tau} = \sum_{k \neq \phi} \frac{\gamma_k}{\gamma} \mathcal{D}[\hat{b}_k] \hat{\rho}(\tau) + \frac{1}{\gamma} [\mathcal{J}\hat{\rho} - i(\hat{H}_{\text{eff}}\hat{\rho} - \hat{\rho}\hat{H}_{\text{eff}}^\dagger)]$$

$$= (\bar{\mathcal{L}}_d + \mathcal{K})\hat{\rho}(\tau), \tag{E1}$$

where $\mathcal{K}\hat{\rho} = (1/\gamma)[\mathcal{J}\hat{\rho} - i(\hat{H}_{\text{eff}}\hat{\rho} - \hat{\rho}\hat{H}_{\text{eff}}^\dagger)]$ and $\bar{\mathcal{L}}_d = \sum_{k \neq \phi}(\gamma_k/\gamma)\mathcal{D}[\hat{b}_k]$. In the limit of strong nonlocal dissipation $\gamma_k \gg \eta, G$ for all $k \neq \phi$, we can treat $\mathcal{K}$ as a perturbative term. A general solution of the master equation is $\hat{\rho}(\tau) = \mathcal{U}(\tau)\rho(0)$, where the propagator $\mathcal{U}(\tau)$ can be expanded in the Dyson series (B4).

The dissipator $\bar{\mathcal{L}}_d$ is identical to the dominant dissipator for the Kerr-resonator array in the Zeno limit. It targets a unique state $\hat{\rho}_d$ in the reduced Hilbert space of modes $k \neq \phi$. For strong nonlocal dissipation $\gamma_k \gg \eta, G$, the dynamics of the system is constrained to the subspace $\hat{\rho}(\tau) = \hat{\rho}_d \otimes \hat{\rho}_\phi(\tau)$ at all times $\tau \gg 1$ [53]. The dynamics of the reduced density matrix $\hat{\rho}_\phi(\tau)$ is described by the propagator

$$\mathcal{P}_d \mathcal{U}(\tau) \mathcal{P}_d = \mathcal{P}_d + \tau \mathcal{P}_d \mathcal{K} \mathcal{P}_d + \mathcal{O}\left(\frac{\eta^2}{\gamma^2}\right)$$

$$= \mathcal{P}_d + \tau \frac{2}{N}\frac{\eta}{\gamma} \mathcal{D}[\hat{Z}_\phi] \mathcal{P}_d + \mathcal{O}\left(\frac{\eta^2}{\gamma^2}\right), \tag{E2}$$

where $\hat{Z}_\phi = \hat{b}_\phi^2 - \tilde{\zeta}^2$. We used the Dyson series (B4) as well as relation (B6) in the first equality and, in the second equality, we explicitly evaluated the first-order term $\mathcal{P}_d \mathcal{K} \mathcal{P}_d$ using $\mathcal{P}_d \hat{H}_{\text{eff}} \mathcal{P}_d \hat{\rho} = -i(\eta/N)\hat{Z}_\phi^\dagger \hat{Z}_\phi \mathcal{P}_d \hat{\rho}$, $\mathcal{P}_d[(\mathcal{P}_d\hat{\rho}) \hat{H}_{\text{eff}}^\dagger] = i(\eta/N)(\mathcal{P}_d\hat{\rho})\hat{Z}_\phi^\dagger \hat{Z}_\phi$, as well as $\mathcal{P}_d \mathcal{J} \mathcal{P}_d \hat{\rho} = 2(\eta/N)\hat{Z}_\phi(\mathcal{P}_d\hat{\rho})\hat{Z}_\phi^\dagger$. Note that the first-order term in the Dyson series leads to decay toward DFS (11) at times $t \sim N/\eta$ [32]. As a result, it is sufficient to consider the Dyson series only up to the first order in $\mathcal{K}$ as higher-order terms set in at longer times $t \sim \gamma/\eta^2$. This is in contrast to the Zeno dynamics of the Kerr-resonator array, where the first-order term in the Dyson series leads to the unitary dynamics and decay toward the DFS is due to the second-order term.

We now consider that we initially start with a state in the subspace $\hat{\rho}_d \otimes \hat{\rho}_\phi$. The time evolution within this subspace is described by $\hat{\rho}_\phi(\tau) = \text{Tr}_d\{\mathcal{P}_d \mathcal{U}(\tau) \mathcal{P}_d[\hat{\rho}_d \otimes \hat{\rho}_\phi(0)]\}$. We obtain the effective master equation (16) in Lindblad form where we used the Dyson series (E2) and rescaled back time, $t = \tau/\gamma$.

APPENDIX F: DISSIPATIVE GAP IN THE ZENO LIMIT

In this appendix we study the dissipative gap Δ_d in the Zeno limit, which is determined from the spectrum of the effective Liouvillian $\mathcal{L}_\phi$ as the smallest nonvanishing real

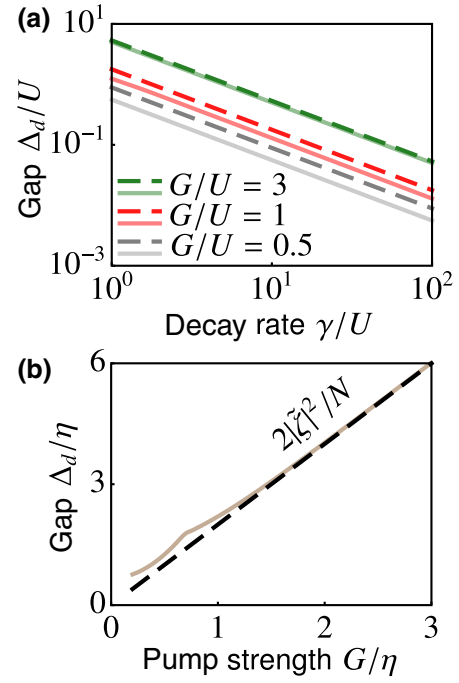FIG. 6. Dissipative gap Δ_d of the effective Liouvillian $\mathcal{L}_\phi$. (a) The dissipative gap of the Kerr-resonator array as a function of the decay rate γ for different values of G/U. The exact values of the dissipative gap obtained by diagonalizing the Liouvillian superoperator (solid lines) and the estimated values of the dissipative gap (dashed lines) according to Eq. (14). (b) The dissipative gap of the alternative model (15) with local two-photon loss as a function of the two-photon pump strength G. (Here $N = 3$ and the truncation is at $M_{k=\phi} = 40$.)

part of the eigenvalues [50]. We investigate the dissipative gap first for the Kerr-resonator array and then for the alternative model with local two-photon loss.

For the Kerr-resonator array, we numerically determine the spectrum of the Liouvillian, and from that we extract the dissipative gap. We plot the dissipative gap in Fig. 6(a) as a function of the nonlocal decay rate γ for several values of the two-photon pump strength G. From the numerical data, we infer that the dissipative gap is $\Delta_d = (\Gamma/2)(N/U)\epsilon_1$, where ϵ_1 is the energy of the first excited state of the effective Hamiltonian $\hat{H}_\phi$. For large $|\zeta| \gtrsim 1$, the energy of the first excited state approaches $\epsilon_1 \approx 4(U/N)|\zeta|^2$ and, as a result, the dissipative gap can be approximated by Eq. (14). In Fig. 6(a), we can see that the exact values (solid lines) approach the values given by Eq. (14) (dashed lines) as the strength G of the two-photon drive and, as a consequence, $|\zeta|$ increase.

We now study the dissipative gap Δ_d for the alternative model, which is extracted from the numerically calculated spectrum of the Liouvillian $\mathcal{L}_\phi$. Note that, in contrast to the Kerr-resonator array, the Liouvillian and, as a consequence, the dissipative gap are independent of γ in the Zeno limit for large γ. We plot the dissipative gap Δ_d

in Fig. 6(b) as a function of the pump power G. It shows that the dissipative gap grows as $\Delta_d \approx 2\eta|\zeta|^2/N$ with the amplitude ζ.

APPENDIX G: EFFECTIVE MASTER EQUATION (18) IN THE PRESENCE OF IMPERFECTIONS

In this appendix, we discuss the effective master equation for mode $q = 1$ for the alternative model (15) with local two-photon loss in the Zeno limit of strong nonlocal dissipation in the presence of imperfections.

To derive the effective master equation in the Zeno limit $\bar{\gamma}_{q\neq1} \gg \eta, G, \bar{\gamma}_1$, we treat terms $\mathcal{K}\hat{\rho} = (1/\gamma)\{\mathcal{L}_\eta + \bar{\gamma}_1 \mathcal{D}[\hat{b}_1]\hat{\rho}\}$ as a perturbation to the dominant dissipation $\bar{\mathcal{L}}_d = \sum_{q\neq1}(\bar{\gamma}_q/\gamma)\mathcal{D}[\hat{b}_q]$. Starting initially in the subspace $\hat{\rho}_d \otimes \hat{\rho}_1$, the dynamics of the reduced density matrix $\hat{\rho}_1$ is described by the effective master equation (18) in Lindblad form within first-order perturbation theory. In the derivation of the effective master equation, we followed the same steps as in Appendix E for the alternative model without imperfections.

The amplitude of cat states $\bar{\zeta}$ and the dissipative gap Δ_d are modified due to disorder in nonlocal decay rates γ_j and jump-operator phases ϕ_j. We plot the distribution of the cat-state amplitude and the dissipative gap in Figs. 7(a) and 7(b), respectively, in the presence of random disorder as a function of the disorder strength σ. We can see that, for moderate disorder $\sigma \lesssim 0.25$, the cat-state amplitude and the dissipative gap retain values that are comparable to those of the disorder-free array for $\sigma = 0$. This is in contrast to the single-photon loss rate $\bar{\gamma}_1$, which reaches considerable values due to even moderate disorder $\sigma \sim 0.25$ and leads to a significant decoherence rate $|\zeta|^2\bar{\gamma}_1$ in comparison to the dissipative gap, as shown in Fig. 5 in the main text.

We plot the distribution of the single-photon loss rate $\bar{\gamma}_1$ and the dissipative gap Δ_d in Figs. 7(c) and 7(d), respectively, for the constant disorder strength $\sigma = 0.075$ as a function of system size N. We can see that the dissipative gap moderately decreases on average (blue dashed

lines) with increasing system size, but it retains values that are comparable to the value $\Delta_d \approx 2G$ of the disorder-free array. The single-photon loss rate moderately increases on average (blue dashed lines) with increasing system size. This is in contrast to the cat-state amplitude $|\zeta|^2 \propto N$ that increases proportionally to system size N, leading to a rapidly increasing decoherence rate $|\bar{\zeta}|^2\bar{\gamma}_1$ as discussed in the main text.

APPENDIX H: SINGLE-PHOTON AMPLIFICATION IN THE PRESENCE OF IMPERFECTIONS

In this appendix, we discuss single-phonon amplification that is a second-order process in $\hat{H}_G$ in the Zeno limit. Crucially, single-photon amplification is the dominant source of decoherence within the DFS for some realizations of disorder in nonlocal dissipation. As a result, single-photon amplification has to be taken into account to accurately describe the dynamics of the selected mode in the Zeno limit.

In particular, we consider the alternative model with vanishing two-photon pump phase $\theta = 0$ [56] and with disordered nonlocal dissipation rates γ_j and jump-operator phases ϕ_j. Within second-order perturbation theory, the dynamics of the selected mode $q = 1$ in the Zeno limit is described by the effective master equation

$$\dot{\hat{\rho}}_1 = 2\frac{\bar{\eta}}{N}\mathcal{D}[\hat{b}_1^2 - \bar{\zeta}^2]\hat{\rho}_1 + \bar{\gamma}_1\mathcal{D}[\hat{b}_1]\hat{\rho}_1 + \mu\mathcal{D}[\hat{b}_1^\dagger]\hat{\rho}_1. \quad (H1)$$

Single-photon amplification at rate

$$\mu = 16G^2 \sum_{j,k=1}^{N} \sum_{q=2}^{N} \frac{T_{j1}^* T_{jq}^* T_{k1} T_{kq}}{\bar{\gamma}_q} \quad (H2)$$

is a second-order process in the two-photon pump $\hat{H}_G$ and is absent within first-order perturbation theory; see Eq. (18).
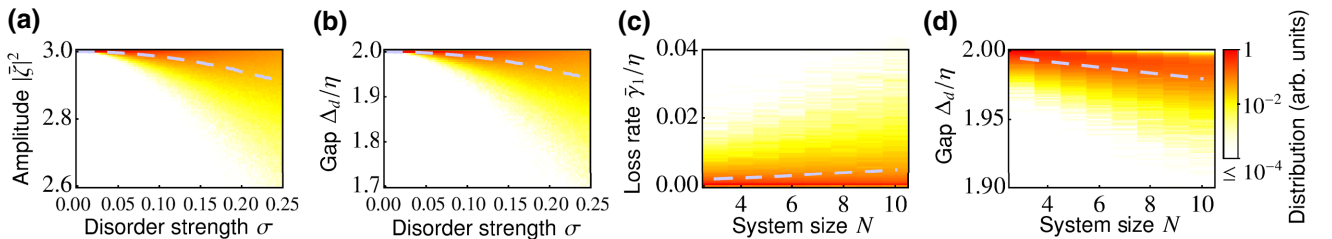

(a) **(b)** **(c)** **(d)**

FIG. 7. Effects of disorder in nonlocal dissipation in the alternative model. Distribution (color gradient) of the the (a) cat-state amplitude $|\zeta|^2$ and (b) dissipative gap Δ_d for disorder in nonlocal decay rates γ_j and jump-operator phases ϕ_j as a function of the disorder strength σ. Distribution (c) of the single-photon loss rate $\bar{\gamma}_1$ and (d) of the dissipative gap as a function of system size N. Blue dashed lines show average values of the corresponding quantities. [Parameters are (a),(b) $N = 3$, $\gamma/\eta = 3$, $G/\eta = 1$; (c),(d) $\sigma = 0.075$, $\gamma/\eta = 4.5/[1 - \cos(2\pi/N)]$, $G/\eta = 1$.]

To derive master equation (H1), we evaluate the second-order term in the Dyson series (B8),

$$\mathcal{P}_d \mathcal{K} \int_0^\tau d\tau_1 \int_0^{\tau_1} d\tau_2 \, e^{\bar{\mathcal{L}}_d(\tau_1-\tau_2)} \mathcal{K} \mathcal{P}_d \approx \frac{\tau}{\gamma} \mu \mathcal{D}[\hat{b}_1^\dagger] \mathcal{P}_d,$$
$$(H3)$$

where we consider only the perturbation in a form of the two-photon pump $\mathcal{K} = -(i/\gamma)[\hat{H}_G, \cdot]$. We neglect the remaining perturbations as they give rise to only marginal second-order corrections.

Single-photon amplification is facilitated by virtual excitations of strongly decaying modes $q \neq 1$. For an ideal array with vanishing jump-operator phases $\phi_j = 0$, the simultaneous excitation of the selected mode $q = 1$ and another mode $q \neq 1$ via the two-photon pump is not allowed due to the conservation of quasimomentum. As a result, the single-photon amplification rate μ vanishes. On the other hand, imperfections in the form of nonvanishing jump-operator phases $\phi_j \neq 0$ lead to the breaking of the quasimomentum conservation. As a consequence, these imperfections enable the simultaneous excitation of the selected mode $q = 1$ and another mode $q \neq 1$, giving rise to nonvanishing single-photon amplification.

We now show that, for imperfections leading to vanishingly small overall phase $\Phi = \sum_{j=1}^N \phi_j$, single-photon amplification is a dominant source of decoherence as the single-photon loss rate $\bar{\gamma}_1$ is negligible. We consider a disordered array with the vanishing overall phase $\Phi = 0$ and, as a consequence, $\bar{\gamma}_1 = 0$. In Fig. 8(a) we plot the fidelity c_{++} of the instantaneous state $\hat{\rho}(t)$ with the even cat state $|\mathcal{C}^+\rangle$ (blue lines) and the fidelity c_{--} with the odd cat state $|\mathcal{C}^-\rangle$ (green lines) as a function of time for different values of the nonlocal dissipation rare γ and starting initially from the vacuum state. In Fig. 8(b), we plot the purity p of the instantaneous state. We can see that at long times the array approaches the fully mixed state $\hat{\rho}_1 \approx \frac{1}{2}(|\mathcal{C}_+\rangle\langle\mathcal{C}_+| + |\mathcal{C}_-\rangle\langle\mathcal{C}_-|)$ with $c_{++} \approx c_{--} \approx p \approx 0.5$ as decoherence due to single-photon amplification sets in. We compare full master equation (15) simulations (dark blue and dark green lines) to the simulations of the effective master equation (H1) in the Zeno limit (light blue and light green lines) and we plot in Fig. 8(b) the difference $\|\hat{\rho} - \hat{\rho}_d \otimes \hat{\rho}_1\|$ (purple lines) between the instantaneous state $\hat{\rho}$ according to the full master equation and the instantaneous state $\hat{\rho}_1$ according to master equation (H1) for the effective Zeno dynamics. We can see that in the Zeno limit for large nonlocal dissipation rate γ, the effective master equation (H1) describes well the time evolution of the array as the difference $\|\hat{\rho} - \hat{\rho}_d \otimes \hat{\rho}_1\|$ is small throughout the entire time evolution.

Single-photon amplification excites the array out of the DFS. As single-photon amplification μ is a second-order processes, it is, in the Zeno limit, weak compared to the two-photon driven dissipation $\bar{\eta}$, which stabilizes the DFS.
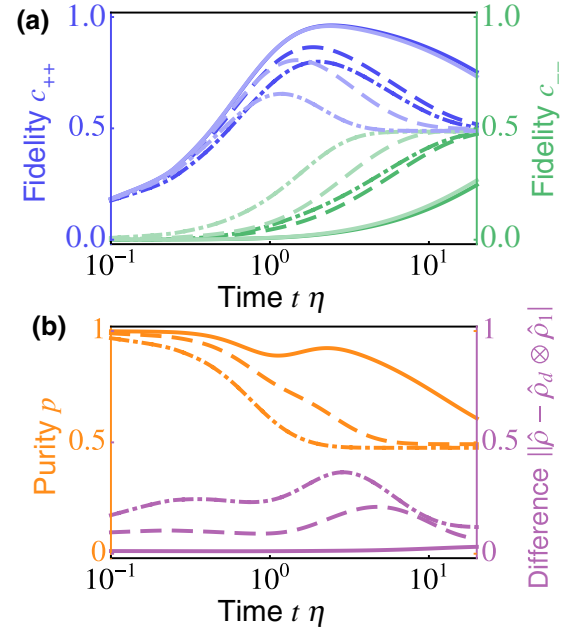

FIG. 8. Effects of single-photon amplification. (a) The fidelity with the even cat state c_{++} (blue lines) and the odd cat state c_{--} (green lines) as a function of time starting initially from the vacuum state for a particular disorder realization with a vanishing overall phase $\Phi = 0$, and for the nonlocal dissipation rate $\gamma/\eta = \sqrt{10}$ (dash-dot lines), $\gamma/\eta = 10$ (dashed lines), and $\gamma/\eta = 10^2$ (solid lines). Full master equation (15) simulations (dark blue and dark green lines) are compared to the simulations of the effective master equation (H1) in the Zeno limit (light blue and light green lines). (b) Purity of the instantaneous state (orange lines) and the difference $\|\hat{\rho} - \hat{\rho}_d \otimes \hat{\rho}_1\|$ (purple lines) between the instantaneous state $\hat{\rho}$ according to the full master equation and the instantaneous state $\hat{\rho}_1$ according to master equation (H1) for the effective Zeno dynamics. (Parameters are $N = 3$, $G/\eta = 1$, $\sigma = 0.1$, $\delta\gamma_1 = 1.34$, $\delta\gamma_2 = 4.59$, $\delta\gamma_3 = -5.65$, $\delta\phi_1 = 2.18$, $\delta\phi_2 = 0.83$, $\delta\phi_3 = -3.00$. Truncation is at $M_{k=\phi} = 18$ and $M_{k\neq\phi} = 3$.)

As a result, upon excitation out of the DFS the array quickly converges back toward the DFS. However, the single-photon amplification process transforms odd-parity eigenstates to even-parity eigenstates and vice versa as it injects a single photon into the array. As a result, single-photon amplification leads to leaking between parity subspaces and convergence toward the fully mixed state.

Even though single-photon amplification leads to decoherence within the DFS, it does not severely limit the fidelity of prepared cat states in the Zeno limit. Since single-photon amplification is a second-order process facilitated by virtual excitations of strongly decaying modes, its rate is inversely proportional to γ; see Eq. (H2). As a result, single-photon amplification is suppressed in the Zeno limit. This is in contrast to single-photon loss whose rate is proportional to γ, leading to strong decoherence in the Zeno limit.

[1] Bastian Hacker, Stephan Welte, Severin Daiss, Armin Shaukat, Stephan Ritter, Lin Li, and Gerhard Rempe, Deterministic creation of entangled atom–light Schrödinger-cat states, Nat. Photonics **13**, 110 (2019).

[2] A. Gilchrist, Kae Nemoto, W. J. Munro, T. C. Ralph, S. Glancy, Samuel L. Braunstein, and G. J. Milburn, Schrödinger cats and their power for quantum information processing, J. Opt. B: Quantum Semiclass. Opt. **6**, S828 (2004).

[3] Vittorio Giovannetti, Seth Lloyd, and Lorenzo Maccone, Advances in quantum metrology, Nat. Photonics **5**, 222 (2011).

[4] Luca Pezzè, Augusto Smerzi, Markus K. Oberthaler, Roman Schmied, and Philipp Treutlein, Quantum metrology with nonclassical states of atomic ensembles, Rev. Mod. Phys. **90**, 035005 (2018).

[5] Brian Vlastakis, Gerhard Kirchmair, Zaki Leghtas, Simon E. Nigg, Luigi Frunzio, S. M. Girvin, Mazyar Mirrahimi, M. H. Devoret, and R. J. Schoelkopf, Deterministically encoding quantum information using 100-photon Schrödinger cat states, Science **342**, 607 (2013).

[6] Christopher Chamberland, K. Noh, P. Arrangoiz-Arriola, E. T. Campbell, C. T. Hann, J. Iverson, H. Putterman, T. C. Bohdanowicz, S. T. Flammia, A. Keller, and G. Refael, Building a fault-tolerant quantum computer using concatenated cat codes, ArXiv:2012.04108 (2020).

[7] A. Grimm, N. E. Frattini, S. Puri, S. O. Mundhada, S. Touzard, M. Mirrahimi, S. M. Girvin, S. Shankar, and M. H. Devoret, Stabilization and operation of a Kerr-cat qubit, Nature **584**, 205 (2020).

[8] Zaki Leghtas, Gerhard Kirchmair, Brian Vlastakis, Robert J. Schoelkopf, Michel H. Devoret, and Mazyar Mirrahimi, Hardware-Efficient Autonomous Quantum Memory Protection, Phys. Rev. Lett. **111**, 120501 (2013).

[9] Mazyar Mirrahimi, Zaki Leghtas, Victor V. Albert, Steven Touzard, Robert J. Schoelkopf, Liang Jiang, and Michel H. Devoret, Dynamically protected cat-qubits: A new paradigm for universal quantum computation, New J. Phys. **16**, 045014 (2014).

[10] Z. Leghtas, S. Touzard, I. M. Pop, A. Kou, B. Vlastakis, A. Petrenko, K. M. Sliwa, A. Narla, S. Shankar, M. J. Hatridge, M. Reagor, L. Frunzio, R. J. Schoelkopf, M. Mirrahimi, and M. H. Devoret, Confining the state of light to a quantum manifold by engineered two-photon loss, Science **347**, 853 (2015).

[11] Nissim Ofek, Andrei Petrenko, Reinier Heeres, Philip Reinhold, Zaki Leghtas, Brian Vlastakis, Yehan Liu, Luigi Frunzio, S. M. Girvin, L. Jiang, Mazyar Mirrahimi, M. H. Devoret, and R. J. Schoelkopf, Extending the lifetime of a quantum bit with error correction in superconducting circuits, Nature **536**, 441 (2016).

[12] Shruti Puri, Samuel Boutin, and Alexandre Blais, Engineering the quantum states of light in a Kerr-nonlinear resonator by two-photon driving, Quantum Inf. **3**, 18 (2017).

[13] Shruti Puri, Alexander Grimm, Philippe Campagne-Ibarcq, Alec Eickbusch, Kyungjoo Noh, Gabrielle Roberts, Liang Jiang, Mazyar Mirrahimi, Michel H. Devoret, and S. M. Girvin, Stabilized Cat in a Driven Nonlinear Cavity: A Fault-Tolerant Error Syndrome Detector, Phys. Rev. X **9**, 041009 (2019).

[14] S. Touzard, A. Grimm, Z. Leghtas, S. O. Mundhada, P. Reinhold, C. Axline, M. Reagor, K. Chou, J. Blumoff, K. M. Sliwa, S. Shankar, L. Frunzio, R. J. Schoelkopf, M. Mirrahimi, and M. H. Devoret, Coherent Oscillations inside a Quantum Manifold Stabilized by Dissipation, Phys. Rev. X **8**, 021005 (2018).

[15] Jérémie Guillaud, and Mazyar Mirrahimi, Repetition Cat Qubits for Fault-Tolerant Quantum Computation, Phys. Rev. X **9**, 041053 (2019).

[16] Shruti Puri, Lucas St-Jean, Jonathan A. Gross, Alexander Grimm, Nicholas E. Frattini, Pavithran S. Iyer, Anirudh Krishna, Steven Touzard, Liang Jiang, Alexandre Blais, Steven T. Flammia, and S. M. Girvin, Bias-preserving gates with stabilized cat qubits, Sci. Adv. **6**, eaay5901 (2020).

[17] Raphaël Lescanne, Marius Villiers, Théau Peronnin, Alain Sarlette, Matthieu Delbecq, Benjamin Huard, Takis Kontos, Mazyar Mirrahimi, and Zaki Leghtas, Exponential suppression of bit-flips in a qubit encoded in an oscillator, Nat. Phys. **16**, 509 (2020).

[18] Shruti Puri, Christian Kraglund Andersen, Arne L. Grimsmo, and Alexandre Blais, Quantum annealing with a network of all-to-all connected, two-photon driven Kerr nonlinear oscillators, Nat. Commun. **8**, 15785 (2017).

[19] Barry C. Sanders, Entangled coherent states, Phys. Rev. A **45**, 6811 (1992).

[20] S. J. van Enk and O. Hirota, Entangled coherent states: Teleportation and decoherence, Phys. Rev. A **64**, 022313 (2001).

[21] Barry C. Sanders, Review of entangled coherent states, J. Phys. A: Math. Theor. **45**, 244002 (2012).

[22] Jaewoo Joo, William J. Munro, and Timothy P. Spiller, Quantum Metrology with Entangled Coherent States, Phys. Rev. Lett. **107**, 083601 (2011).

[23] Y. M. Zhang, X. W. Li, W. Yang, and G. R. Jin, Quantum fisher information of entangled coherent states in the presence of photon loss, Phys. Rev. A **88**, 043832 (2013).

[24] Chen Wang, Yvonne Y. Gao, Philip Reinhold, R. W. Heeres, Nissim Ofek, Kevin Chou, Christopher Axline, Matthew Reagor, Jacob Blumoff, K. M. Sliwa, L. Frunzio, S. M. Girvin, Liang Jiang, M. Mirrahimi, M. H. Devoret, and R. J. Schoelkopf, A Schrödinger cat living in two boxes, Science **352**, 1087 (2016).

[25] Samuel L. Braunstein and Peter van Loock, Quantum information with continuous variables, Rev. Mod. Phys. **77**, 513 (2005).

[26] Xiaoguang Wang and Barry C. Sanders, Multipartite entangled coherent states, Phys. Rev. A **65**, 012303 (2001).

[27] Alexandre Blais, Steven M. Girvin, and William D. Oliver, Quantum information processing and quantum optics with circuit quantum electrodynamics, Nat. Phys. **16**, 247 (2020).

[28] Alexandre Blais, Arne L. Grimsmo, S. M. Girvin, and Andreas Wallraff, Circuit quantum electrodynamics, Rev. Mod. Phys. **93**, 025005 (2021).

[29] Wen-Long Ma, Shruti Puri, Robert J. Schoelkopf, Michel H. Devoret, S. M. Girvin, and Liang Jiang, Quantum control of bosonic modes with superconducting circuits, Sci. Bull. **66**, 1789 (2021).

[30] J. F. Poyatos, J. I. Cirac, and P. Zoller, Quantum Reservoir Engineering with Laser Cooled Trapped Ions, Phys. Rev. Lett. **77**, 4728 (1996).

[31] A. Metelmann and A. A. Clerk, Nonreciprocal Photon Transmission and Amplification via Reservoir Engineering, Phys. Rev. X **5**, 021025 (2015).

[32] L. Gilles, B. M. Garraway, and P. L. Knight, Generation of nonclassical light by dissipative two-photon processes, Phys. Rev. A **49**, 2785 (1994).

[33] M. Mamaev, L. C. G. Govia, and A. A. Clerk, Dissipative stabilization of entangled cat states using a driven Bose-Hubbard dimer, Quantum **2**, 58 (2018).

[34] Diego Porras and Samuel Fernández-Lorenzo, Topological Amplification in Photonic Lattices, Phys. Rev. Lett. **122**, 143901 (2019).

[35] Clara C. Wanjura, Matteo Brunelli, and Andreas Nunnenkamp, Topological framework for directional amplification in driven-dissipative cavity arrays, Nat. Commun. **11**, 3149 (2020).

[36] Vincenzo Savona, Spontaneous symmetry breaking in a quadratically driven nonlinear photonic lattice, Phys. Rev. A **96**, 033826 (2017).

[37] Riccardo Rota, Fabrizio Minganti, Cristiano Ciuti, and Vincenzo Savona, Quantum Critical Regime in a Quadratically Driven Nonlinear Photonic Lattice, Phys. Rev. Lett. **122**, 110405 (2019).

[38] Hayato Goto, Bifurcation-based adiabatic quantum computation with a nonlinear oscillator network, Sci. Rep. **6**, 21686 (2016).

[39] Simon E. Nigg, Niels Lörch, and Rakesh P. Tiwari, Robust quantum optimizer with full connectivity, Sci. Adv. **3**, e1602273 (2017).

[40] B. Kraus, H. P. Büchler, S. Diehl, A. Kantian, A. Micheli, and P. Zoller, Preparation of entangled states by quantum Markov processes, Phys. Rev. A **78**, 042307 (2008).

[41] Phases ϕ and θ are connected by the local gauge transformation $\hat{a}_j \rightarrow \hat{a}_j e^{ij\nu}$, yielding $\phi \rightarrow \phi + \nu$ and $\theta \rightarrow \theta + 2\nu$. While these phases are gauge dependent, the phase difference $2\phi - \theta$ is gauge invariant. For $2\phi - \theta = 0$ (corresponding to $\theta = 2\phi$ set in the main text), we are able to express the dark state condition in the form of Eq. (9), allowing us to write exact closed-form solutions for the dark states.

[42] Zhaoyou Wang, Marek Pechal, E. Alex Wollack, Patricio Arrangoiz-Arriola, Maodong Gao, Nathan R. Lee, and Amir H. Safavi-Naeini, Quantum Dynamics of a Few-Photon Parametric Oscillator, Phys. Rev. X **9**, 021049 (2019).

[43] B. Wielinga and G. J. Milburn, Quantum tunneling in a Kerr medium with parametric pumping, Phys. Rev. A **48**, 2494 (1993).

[44] Equation (12) can be derived using $|\pm\zeta\rangle = \mathcal{D}_{\hat{b}_\phi}(\pm\zeta)|0\rangle$ and $\mathcal{D}_{\hat{b}_\phi}(\pm\zeta) = \prod_{j=1}^{N} \mathcal{D}_{\hat{a}_j}(\pm\zeta_j)$, which follows from $\hat{b}_k = (1/\sqrt{N}) \sum_{j=1}^{N} e^{ijk}\hat{a}_j$ and $[\hat{a}_j, \hat{a}_m^\dagger] = \delta_{jm}$, where $\mathcal{D}_{\hat{c}}(\zeta) = \exp(\zeta\hat{c}^\dagger - \zeta^*\hat{c})$ is the displacement operator and $|0\rangle = \bigotimes_{j=1}^{N}|0\rangle_j = \bigotimes_k|0\rangle_k$ is the N-mode vacuum state.

[45] Nadeem A. Ansari and V. I. Man'ko, Squeezing in multimode Schrödinger cat states, J. Russ. Laser Res. **15**, 377 (1994).

[46] W. Vogel and J. Sperling, Unified quantification of nonclassicality and entanglement, Phys. Rev. A **89**, 052302 (2014).

[47] H. Jeong and M. S. Kim, Efficient quantum computation using coherent states, Phys. Rev. A **65**, 042305 (2002).

[48] The joint Wigner function of the N-mode state $\hat{\rho}$ is $W(\vec{x}, \vec{p}) = \pi^{-N} \int_{\mathbb{R}^N} d\vec{y} \exp(-2i\vec{y} \cdot \vec{p})\langle\vec{x} + \vec{y}|\hat{\rho}|\vec{x} - \vec{y}\rangle$, where $\vec{x}, \vec{p}$, and $\vec{y}$ are real-valued N-dimensional vectors, and x_j and p_j are quadratures of resonator j. For cat states stabilized in mode $\phi \neq 0$, the amplitudes ζ_j and ζ_{j+1} at neighboring resonators have a relative phase difference ϕ [see Eq. (12)]. This results in a relative rotation between the local coherent states $|\zeta_j\rangle_j$ and $|\zeta_{j+1}\rangle_{j+1}$ in phase space by an angle ϕ.

[49] Note that the dynamics of an array with only two resonators, i.e., $N = 2$, is fundamentally different from that of larger arrays with $N \geq 3$ as the photon parity $\hat{\mathcal{P}}_\phi = \exp(i\pi\hat{b}_\phi^\dagger\hat{b}_\phi)$ of mode ϕ is conserved, where the quasimomentum can take only values $\phi = 0, \pi$. As a result, the even-parity cat state $|\mathcal{C}^+\rangle$ is deterministically approached from the initial vacuum state for any γ. However, in this manuscript we focus on arrays $N \geq 3$ for which the photon parities $\hat{\mathcal{P}}$ and $\hat{\mathcal{P}}_\phi$ are not conserved.

[50] Victor V. Albert and Liang Jiang, Symmetries and conserved quantities in Lindblad master equations, Phys. Rev. A **89**, 022118 (2014).

[51] B. Misra and E. C. G. Sudarshan, The Zeno's paradox in quantum theory, J. Math. Phys. **18**, 756 (1977).

[52] Kazuki Koshino and Akira Shimizu, Quantum Zeno effect by general measurements, Phys. Rep. **412**, 191 (2005).

[53] Vladislav Popkov, Simon Essink, Carlo Presilla, and Gunter Schütz, Effective quantum Zeno dynamics in dissipative quantum systems, Phys. Rev. A **98**, 052110 (2018).

[54] Gerhard Kirchmair, Brian Vlastakis, Zaki Leghtas, Simon E. Nigg, Hanhee Paik, Eran Ginossar, Mazyar Mirrahimi, Luigi Frunzio, S. M. Girvin, and R. J. Schoelkopf, Observation of quantum state collapse and revival due to the single-photon Kerr effect, Nature **495**, 205 (2013).

[55] The dissipator $\mathcal{L}_\gamma\hat{\rho} = \sum_{j,l=1}^{N} D_{jl}[\hat{a}_j\hat{\rho}\hat{a}_l^\dagger - \frac{1}{2}\{\hat{a}_l^\dagger\hat{a}_j, \hat{\rho}\}] = \sum_{q=1}^{N} \bar{\gamma}_q[\hat{b}_q\hat{\rho}\hat{b}_q^\dagger - \frac{1}{2}\{\hat{b}_q^\dagger\hat{b}_q, \hat{\rho}\}]$ can always be diagonalized by the linear transformation T_{jq} of annihilation operators, where columns of the transformation matrix T_{jq} and single-photon loss rates $\bar{\gamma}_q$ are eigenvectors and eigenvalues, respectively, of the dynamical matrix D_{jl}.

[56] Jump-operator phases $\phi_j \rightarrow \phi_j + \nu_j - \nu_{j+1}$ and two-photon pump phases $\theta_j \rightarrow \theta_j + 2\nu_j$ transform under the local gauge transformation $\hat{a}_j \rightarrow \hat{a}_j e^{i\nu_j}$. Master equation (15) with vanishing two-photon pump phases $\theta_j = 0$ for all j describes a general situation with any two-photon pump phases $\theta_j \neq 0$ (that can also vary at different resonators j) for the particular gauge choice $\nu_j = -\theta_j/2$.

[57] Matthew Reagor, Hanhee Paik, Gianluigi Catelani, Luyan Sun, Christopher Axline, Eric Holland, Ioan M. Pop, Nicholas A. Masluk, Teresa Brecht, Luigi Frunzio, Michel H. Devoret, Leonid Glazman, and Robert J. Schoelkopf, Reaching 10 ms single photon lifetimes for superconducting aluminum cavities, Appl. Phys. Lett. **102**, 192604 (2013).

[58] Matthew Reagor, Wolfgang Pfaff, Christopher Axline, Reinier W. Heeres, Nissim Ofek, Katrina Sliwa,

Eric Holland, Chen Wang, Jacob Blumoff, Kevin Chou, Michael J. Hatridge, Luigi Frunzio, Michel H. Devoret, Liang Jiang, and Robert J. Schoelkopf, Quantum memory with millisecond coherence in circuit QED, Phys. Rev. B **94**, 014506 (2016).

[59] K. M. Sliwa, M. Hatridge, A. Narla, S. Shankar, L. Frunzio, R. J. Schoelkopf, and M. H. Devoret, Reconfigurable Josephson Circulator/Directional Amplifier, Phys. Rev. X **5**, 041020 (2015).

[60] F. Lecocq, L. Ranzani, G. A. Peterson, K. Cicak, R. W. Simmonds, J. D. Teufel, and J. Aumentado, Nonreciprocal Microwave Signal Processing with a Field-Programmable Josephson Amplifier, Phys. Rev. Appl. **7**, 024028 (2017).

[61] Young-Sik Ra, Adrien Dufour, Mattia Walschaers, Clément Jacquard, Thibault Michel, Claude Fabre, and Nicolas Treps, Non-Gaussian quantum states of a multimode light field, Nat. Phys. **16**, 144 (2020).

[62] Wojciech Hubert Zurek, Decoherence, einselection, and the quantum origins of the classical, Rev. Mod. Phys. **75**, 715 (2003).

[63] Zejian Li, Ariane Soret, and Cristiano Ciuti, Dissipation-induced antiferromagneticlike frustration in coupled photonic resonators, Phys. Rev. A **103**, 022616 (2021).

[64] Zheng-Yang Zhou, Clemens Gneiting, J. Q. You, and Franco Nori, Generating and detecting entangled cat states in dissipatively coupled degenerate optical parametric oscillators, Phys. Rev. A **104**, 013715 (2021).

[65] See Supplemental Material at http://link.aps.org/supplemental/10.1103/PRXQuantum.3.010301 for the explicit evaluation of the second-order term in the Dyson series (B8).